ACCSCIENCE PUBLISHING
An International Journal of Optimization and Control: Theories & Applications
ISSN: 2146-0957 eISSN: 2146-5703
Vol.16, No.1, pp.111-137 (2026)
https://doi.org/10.36922/IJOCTA025220107

RESEARCH ARTICLE

A novel fractional-order model with data-driven validation for the dynamics of complex epidemic spreading in networks

Mahmoud Rokaya[1*], Dalia I. Hemdan[2], Mohammed A. Alzain[1], and El-Sayed Atlam[3,4]

[1]Department of Information Technology, College of Computers and Information Technology, Taif University, Taif, Makkah, Saudi Arabia
[2]Department of Food Science and Nutrition, Faculty of Science, Taif University, Taif, Makkah, Saudi Arabia
[3]Department of Computer Science, College of Computer Science and Engineering, Taibah University, Yanbu, Medina, Saudi Arabia
[4]Department of Computer Science, Faculty of Science, Tanta University, Tanta, Gharbia, Egypt
mahmoudrokaya@tu.edu.sa, dalia.m@tu.edu.sa, m.alzain@tu.edu.sa, satlam@taibahu.edu.sa

ARTICLE INFO

Article History:
Received: May 29, 2025
1st revised: August 3, 2025
2nd revised: September 19, 2025
Accepted: October 9, 2025
Published Online: November 22, 2025

Keywords:
Fractional calculus
Epidemic modeling
Physics-informed neural networks
Reinforcement learning
Optimal control
Real-world validation
Data fairness

AMS Classification 2010:
90B23, 90B56

ABSTRACT

Mathematical modeling of epidemics is a cornerstone in the study and response to the spread of diseases and related processes across various domains. However, classical models generally do not describe such memory effects properly and are computationally inefficient, which restricts their applicability or predictive accuracy. To address these issues, we introduce a new approach to epidemic modeling using our newly proposed fractional-order differential equations, which are endowed with the Atangana–Baleanu system to describe long-range dependencies and nonlinear characteristics more accurately than the traditional Caputo system. To address this, we develop physics-informed neural networks and Fourier-based artificial intelligence-driven surrogate solvers, which are computationally efficient without compromising accuracy. To actuate intervention policies in a dynamic fashion, we also incorporate a hybrid control mechanism integrating the use of reinforcement learning with classical mathematical optimization to facilitate adaptive policymaking that benefits from data. Unlike existing work, our framework is rigorously evaluated on real-world epidemiological datasets from the World Health Organization and the Centers for Disease Control and Prevention, and tested extensively for out-of-the-box adaptability to cybersecurity (cyber malware), social rumor, and financial contagion problems. We also propose a data-free generative model (Fair4Free) that improves fairness, privacy, and utility in synthetic dataset generation, allowing its use even for constrained-data settings. Experimental evidence indicates that our holistic approach enhances the accuracy of predictive performance compared to baselines, with both lower computational cost and cross-domain generalizability to unprecedented settings. Finally, we set a new state-of-the-art for EpiModel by end-to-end training on fair data.

1. Introduction

Modeling mathematics has played a crucial role in identifying and predicting the spread of diseases across various fields and situations, as well as detecting security breaches related to cybersecurity and financial contagion due to an epidemic. Mathematical modeling has become an important tool for analyzing and forecasting dynamics beyond traditional timescales. Classical models, such as the susceptible–infected–recovered (SIR) model, [1,2] have laid the foundations of knowledge in this field. However, they build on idealized conditions—for example, mixing populations that are homogeneous or transmission rates with spatially static features according to one's location—and so do not accurately reflect reality in every

*Corresponding Author

case. To overcome these limitations, fractional-order differential equations (FODEs) have been increasingly used. [3–5] These equations capture memory effects and non-local interactions, necessary conditions for describing the long-term behavior of systems that are anything but evenly distributed. These advances make epidemic modeling more realistic and adaptable in both biological and artificial networks.

Following the breakthroughs of traditional models, recent progress blends artificial intelligence (AI) techniques with fractional-order modeling to enhance the precision, scalability, and practical relevance of epidemic forecasting. For example, Raza et al. [6] employed AI computation for solving a fractional-order COVID-19 model that exhibits AI's unique capability to handle both nonlinearity and memory effects. Building on this integration, Cai et al. [7] incorporated fractional physics-informed neural networks (PINNs) to susceptible–exposed–infectious–recovered (SEIR) models to better predict the Omicron wave. Further, Kharazmi et al. [8] used PINNs to learn integer and fractional-order epidemiological models of illness and demonstrated their monopoly on detecting implicit dynamics without solvers. Despite these innovations, current methods frequently remain confined within specific domains and do not generalize well to heterogeneous data sets or real-world situations, an issue directly addressed by our proposed approach. In spite of recent progress, there are still critical failures of current epidemic modeling frameworks that impede practical deployment:

(i) Memory effects: Integer-order models cannot adequately represent historical dependencies of disease dynamics, [9,10] which results in poor long-term forecasting performance.

(ii) Computational bottlenecks: Real-time decision support is a must in dynamically evolving conditions, such as high-dimensional fractional-order systems, but these problems are notoriously expensive to solve. [11]

(iii) Lacking real-world validation: Models often partially validated on synthetic or field-specific data, these papers have yet to be validated further in a demanding real-world context, such as public health, cybersecurity, or the financial world at large.

(iv) Domain rigidity: Although contagion processes cross multiple domains, from computer viruses to disinformation campaigns to stock market crashes, most of this research is pursued separately across different domains. All of these put real limits on how effective models can be generalized from one field to another. [2]

To overcome these constraints, the current study introduces a unified framework. This framework merges cutting-edge fractional-order epidemic models with AI-augmented solutions and in-depth validation for the public health, cybersecurity, and financial domains:

- Mathematical fundamentals: The model is based on Atangana–Baleanu and Caputo–Fabrizio fractional derivatives, which allow memory-dependent transmission processes and stochastic dynamics to be considered. Thus, the model could better simulate the uncertainties seen in real-world contagion events. Time-vectored parameters and noise components further enable the potential of this system to properly replicate random trajectories of real-world infections.
- AI-augmented solutions: We apply PINNs and Fourier neural operators (FNOs) to solve the underlying FODEs outside standard grid systems. These solutions, though heavily used in partial differential equation modeling, represent a rich source of research data within multi-domain disease situations. Our research fills this important gap by adapting such methods adequately to large-scale epidemic datasets and heterogeneous multi-domain databases.
- Evaluation in multiple real-world domains: We encapsulate our comprehensive empirical validation strategy. Unlike early works mostly carried out with synthetic data alone, our methods have been validated against a wide range of real-world datasets. Our model has been applied to World Health Organization (WHO) and Centers for Disease Control and Prevention (CDC) infection numbers, and also put up against Cyberspace to test whether our method is workably safe and mathematically compelling on Wall Street. [17] This emphasizes that it is amenably scalable and context-aware.

The novel blend of precise numbers, AI scalability, and empirical test equipment is crystal clear. It addresses concerns previously mentioned about how realistic research looks at one location compared to another on the map; worries that

results from one location remain valid for people elsewhere in a world where things are constantly changing.

We propose a unified modeling paradigm that combines fractional-order epidemic models with AI-based numerical solvers and empirically validated performance metrics. This integrated framework improves predictive accuracy and computational efficiency while enabling cross-domain adaptability. In addition, we introduce a cooperative module named Fair4Free to address challenges related to data scarcity, privacy, and fairness in the generation of synthetic data. The method involves a data-free distillation process from a teacher model that generates fair latent representations, followed by a student model capable of producing high-fidelity synthetic datasets without exposing sensitive information. This approach ensures both privacy preservation and applicability across diverse domains. With thorough evaluation on tabular and image datasets, Fair4Free outperforms existing state-of-the-art approaches in terms of accuracy, fairness preservation, and usability.

With its thorough evaluation on both tabular and image datasets, Fair4Free notably outperforms current state-of-the-art approaches in terms of accuracy, fairness preservation, and usability. At this stage, these advances made analysis of epidemic forecasting by AI-enhanced fractional models and the new components in its historic system from privacy-preserving synthetic data generation more pertinent.

2. Methods

2.1. Mathematical model and artificial intelligence-based computational framework for epidemic modeling

2.1.1. Introduction to epidemic dynamics

In a realistic epidemic scenario, the infection among individuals is not instantaneous; the pathogens are also not always infectious when they start transmitting. Rather, it is shaped by previous exposures, pathogens that persist in the environment, and the specific network of social or system-based interactions that lies behind transmission. Conventional epidemic models generally assume that infections come from instantaneous contacts, an oversimplification that real-world cases do not support. To break free from these constraints, we combine two vital features and produce a more realistic approach:

i. The use of fractional-order derivatives with long-term memory effects in transmission dynamics; and

ii. The incorporation of network-based propagation mechanisms to capture structured interactions among individuals, systems, or environments.

Our model has the advantage of better capturing complex epidemic behavior, such as latency, non-local exposure, and indirect routes. Fractional-order derivatives enable the modeling of memory effects in transmission dynamics. They quantify how previous exposures are reflected in present transmission states, just like a derivative characterizes current change. Unlike standard derivatives, however, fractional derivatives transfer historical information into real-time dynamics, enabling numerical simulations to exhibit greater realism for epidemic processes.

Real-world interactions operate on structured topologies, such as social, informational, or financial networks, where connections are non-uniform and directional. We, therefore, adopt a network-based propagation framework, where nodes represent agents or subsystems and directed or weighted edges convey interaction pathways. This allows the model to simulate how outbreaks can spread through interconnected and heterogeneous populations.

We considered a hybrid structure that combines both Atangana–Baleanu–Caputo and Caputo fractional operators to better reflect the complex memory aspects of real-world scenarios. This approach aligns with recent studies into coupled hybrid systems involving non-uniform fractional orders. [18,19]

Recent advances in fractional calculus have emphasized the role of fractional differential systems with delays in capturing memory and hereditary properties of physical and biological processes. In particular, fractional integrodifferential systems of order $1 < r < 2$ with Sobolev-type structures are increasingly applied in modeling fluid flow in fissured media, thermodynamics, and viscoelastic materials. [20] Ma et al. [20] rigorously investigated the approximate controllability of such systems under infinite delay by combining Caputo fractional derivatives, Sobolev-type formulations, cosine families, and Martelli's fixed point theorem. They established the existence of mild solutions and proved approximate controllability under well-defined assumptions, including compactness of operator families and Carathéodory conditions. These results extend earlier work on fractional systems of order $0 < r < 1$, highlighting how Sobolev-type integrodifferential inclusions guarantee controllability even with infinite delays. This line of research provides a mathematically validated pathway for

applying fractional-order models in engineering and applied sciences. It directly motivates the use of fractional-order frameworks in our epidemic modeling approach. [20]

2.1.2. Theoretical framework for deriving equations for epidemics

We divide the population into different groups to accurately describe the spread of the epidemic. These groups include:

(i) People who have not yet been infected but are susceptible.
(ii) The group of infected individuals, which includes carriers and spreaders of the disease.
(iii) Recovered individuals are those who successfully combated the virus but may lose immunity and become susceptible again.

We also introduce an external transmission factor that reflects environmental contamination, persistent cybersecurity vulnerabilities, or vectors of misinformation. Since past events affect the present, we model the dynamics of each of these groups as differential equations with a fractional system, accounting for memory effects. According to the Atangana–Baleanu and Caputo–Fabrizio definitions, the general form of the fractional derivative is shown in Equation (1).

$$ {}_0^C D_t^\gamma f(t) = \frac{1-\gamma}{\Gamma(1-\gamma)} \int_0^t \frac{f(\tau)}{(t-\tau)^\gamma} d\tau \qquad (1) $$

where, t represents the current time variable, τ denotes the historical (memory) integration variable, and Γ is the Gamma function used for normalization; meanwhile, $0 < \gamma \leq 1$ denotes the fractional-order parameter that governs the significance of past states in influencing the present. This formulation, which follows the Atangana–Baleanu and Caputo–Fabrizio definitions, offers a more biologically realistic approach to modeling memory-dependent dynamics in complex epidemic systems. We adopt incommensurate fractional derivatives to enhance the system's ability to model scale-specific diffusion and memory behaviors. [21]

New individuals are continuously added to the susceptible population through recruitment (e.g., birth or immigration). However, this compartment is also diminished through direct infection, natural removal (aging or unrelated death), and loss of acquired immunity. A person can contract the infection through direct exposure to infected individuals or via external infection channels (e.g., environmental contamination or cyber infiltration). Equation (2) shows the governing equation for the susceptible population.

$$ \begin{aligned} {}_0^C D_t^\gamma S(t) = \Lambda - \delta S(t) - \sum_j \Big(\frac{\beta_{ij} S(t) I_j(t)}{N} \\ -\lambda S(t) E(t)\Big) + \nu R(t) \end{aligned} \qquad (2) $$

where Λ on the right corresponds to new recruitments into the susceptible population, while $\delta S(t)$ encompasses natural removal from aging or other external causes. The $\beta_{ij} S(t) I_j(t) - \lambda S(t) E(t)$ describes direct transmission, as the rate of infection directly depends on the network structure and the strength of interactions, modeled as β_{ij}. Four external infections are from exposures, such as the external environment, contamination, misinformation, and cybersecurity. The $\upsilon R(t)$ considers recovered individuals losing their immunity and entering the susceptible compartment.

The infected population grows as susceptible individuals become infected either through direct contact or through environmental or external factors. It declines due to recovery, disease-induced mortality, or natural causes. These dynamics are modeled by the following fractional-order differential Equation (3):

$$ \begin{aligned} {}_0^C D_t^\gamma I(t) = \sum_j \beta_{ij} S(t) I_j(t) + \lambda S(t) E(t) \\ -(\nu + \alpha + \delta) I(t) \end{aligned} \qquad (3) $$

where, $\beta_{ij} S(t) I_j(t)$ denotes network-based infection transmission, while $\lambda E(t) S(t)$ represents external or environmental infection exposure. The remaining terms $R(t)$, $\alpha I(t)$, and $\delta S(t)$ correspond to recovery, disease-induced death, and natural death, respectively.

The recovered population consists of individuals who have successfully overcome the infection. However, immunity is not always permanent, and some may revert to a susceptible state. This dynamic is described using the following fractional differential Equation (4):

$$ {}_0^C D_t^\gamma R(t) = \alpha I(t) - \nu R(t) \qquad (4) $$

The term $\alpha I(t)$ accounts for the transition of infected individuals into the recovered group, while $\nu R(t)$ represents the rate at which recovered individuals lose immunity and become susceptible again.

To capture external influences that contribute to the spread of infection—such as contaminated surfaces, persistent misinformation, or sustained

cyber vulnerabilities—we introduce an environmental or external compartment governed by the following Equation (5):

$$ {}_0^C D_t^\gamma E(t) = Q(P) - g_0 E(t) \tag{5} $$

where, $Q(P)$ denotes the external epidemic accelerants, which may include misinformation campaigns, environmental contamination, or coordinated cyberattacks. The decay term $g_0 E(t)$ represents mitigation processes, such as disinfection, fact-checking, or cybersecurity measures, that reduce the impact of such external factors over time. This helps in reconstructing latent epidemic states from partial data and aligns with the theoretical foundation of time-fractional systems. [22] This structure reflects real-world biological processes with nested memory layers and requires analyzing the coupled dynamics. [23]

2.1.3. Epidemic spread modeling in a network

In real life, infections are not stochastic in most cases. Instead, they follow arbiter pathways along social networks, financial interactions, or digital connections. To model this, we introduce an adjacency matrix, A_{ij}, wherein each element indicates the connection between two nodes. For an individual to be infectious, it depends on their network position and the connections they have. This is expressed as Equation (6) given below:.

$$ {}_0^C D_t^\gamma I_i = \sum_j \beta_{ij} \Lambda_{ij} S_i I_j - (\nu_i + \alpha_i + \delta_i) I_i \tag{6} $$

This equation ensures that infections only spread via actual connections, as opposed to uniformly transmitting across the population.

2.2. Theoretical derivation of the fractional-order epidemic model

To capture the long-term dependencies that characterize epidemic transmission, we adopt a fractional-order modeling approach using the Atangana–Baleanu derivative in the Caputo sense. This derivative incorporates memory effects and is defined in Equation (7) given below:

$$ {}_0^{ABC} D^\alpha f(t) = \frac{B(\alpha)}{1-\alpha} \int_0^t f^t(\tau) E_\alpha \left(-\frac{\alpha}{1-\alpha} (t-\tau)^\alpha \right) d\tau, \tag{7} $$

where $0 < a < 1$ is the fractional order, $B(a)$ is a normalization constant to maintain consistency with standard derivatives as $\alpha \to 1$, and $E_\alpha(\ldots)$ denotes the Mittag–Leffler function, which generalizes the exponential function to model memory and hereditary properties observed in complex systems. [24]

To simulate the dynamics of epidemic transmission, we segment the population into the following compartments at each node i:

- $S_i(t)$: Susceptible individuals not yet infected but vulnerable to exposure.
- $I_i(t)$: Infected individuals actively transmitting the disease or disturbance.
- $R_i(t)$: Recovered individuals who may have developed temporary immunity.
- Additionally, we define an external factor $E(t)$ to represent indirect transmission sources, such as environmental contamination, latent cybersecurity vulnerabilities, or misinformation propagation. Given that past exposures influence future states, the evolution of these compartments is governed by FODEs.

These equations embed memory effects through operators, such as the Atangana–Baleanu and Caputo–Fabrizio derivatives. To reflect structured interactions, we introduce an adjacency matrix A_{ij} where each entry denotes the presence or absence of a connection between nodes i and j. The parameter N denotes the total population size.

The full system of equations governing the fractional-order epidemic dynamics begins with the susceptible population, which changes due to recruitment, natural removal, direct and indirect infections, and the reversal of immunity loss. The equation is shown in Equation (8) as given below:

$$ {}_0^{ABC} D_t^\alpha S_i(t) = \Lambda - \mu S_i(t) - \beta \sum_{j=1}^{N} \left(\frac{A_{ij} S_i(t) I_j(t)}{N} \right) - \lambda E(t) S_i(t) + \nu R_i(t) \tag{8} $$

where:

- Λ denotes the rate of new susceptible individuals entering the population,
- μ is the natural mortality rate,
- β is the infection transmission coefficient,
- λ quantifies the effect of external influences such as environmental persistence or misinformation,
- v accounts for the re-entry of recovered individuals due to immunity waning.

The infected population increases due to infections acquired through both direct contact and external sources, while it decreases through recovery, disease-induced death, and natural mortality.

This is formulated as Equation (9) given below:

$$\begin{aligned} {}_0^{ABC}D_t^{\alpha} I_i(t) = \beta \sum_{j=1}^{N} \left(\frac{A_{ij} S_i(t) I_j(t)}{N}\right) \\ -\lambda E(t) S_i(t) - (\gamma + \delta + \mu) I_i(t) \end{aligned} \tag{9}$$

In this equation,

- β represents the direct infection rate,
- λ captures the contribution of external environmental factors,
- γ is the recovery rate,
- δ is the mortality due to the disease itself, and
- μ reflects natural death.

The recovered population increases as infected individuals survive the illness, but may decrease over time due to loss of immunity or natural death. This is expressed as Equation (10) given below:

$${}_0^{ABC}D^{\alpha} R_i(t) = \gamma I_i(t) - (\nu + \mu) R_i(t) \tag{10}$$

where, γ denotes the rate at which individuals recover from infection, v represents the rate of waning immunity returning individuals to the susceptible pool, and μ accounts for natural mortality among the recovered. Our framework incorporates parameter optimization and control tuning through stochastic approaches. [25]

To model external drivers of infection, such as lingering contamination, misinformation campaigns, or latent cybersecurity threats, we define an external compartment governed by Equation (11).

$${}_0^{ABC}D^{\alpha} E(t) = \theta \sum_{i=1}^{N} I_i(t) - \delta_e E(t) \tag{11}$$

where:

- θ captures the influence of infected individuals in amplifying the external transmission factor.
- δ_e denotes the decay rate of this factor due to mitigation efforts like environmental cleaning, public awareness, or cyberdefense mechanisms.

This reflects the combination of structured interactions, environmental persistence, and memory effects that can characterize reality and that make long-term disease modeling more realistic. [26]

2.2.1. Physics-informed neural networks

To solve the fractional-order epidemic system while enforcing the physical laws embedded in its structure, we employ PINNs. [27] The neural network is trained to estimate the compartmental trajectories as shown in Equation (12) given below:

$$\mathcal{NN}_{\theta(t)} == \left(\widehat{S}_i(t), \widehat{I}_i(t), \widehat{R}_i(t), \widehat{E}(t)\right) \tag{12}$$

where θ denotes the trainable parameters of the network. The training objective minimizes a composite loss function that integrates both observational data and the underlying physics of the system Equation (13).

$$\mathcal{L} = \mathcal{L}_{data} + \mathcal{L}_{physics} \tag{13}$$

This dual-objective formulation ensures that the model aligns with real-world data while remaining consistent with the FODEs that govern the system's evolution. [28]

For data loss, this component of the loss function guarantees fidelity to available real-world observations. It penalizes the difference between predicted and observed values across all compartments Equation (14). [29]

$$\begin{aligned} \mathcal{L}_{data} = \sum_{k} \Bigg(\left|\widehat{S}_i(t_k) - S_i^{data}(t_k)\right|^2 \\ + \left|\widehat{I}_i(t_k) - I_i^{data}(t_k)\right|^2 \\ + \left|\widehat{R}_i(t_k) - R_i^{data}(t_k)\right|^2 \\ + \left|\widehat{E}(t_k) - E^{data}(t_k)\right|^2 \end{aligned} \tag{14}$$

Each term reflects the squared error between the network's prediction and the corresponding ground truth for a given timestamp t_k, ensuring data consistency throughout the learning process. For physics-informed loss, this term enforces consistency between the network's predictions and the governing fractional-order epidemic dynamics using the Atangana–Baleanu operator Equation (15).

$$\mathcal{L}_{physics} = \sum_{k} \Big(\Big| {}^{ABC}D^{\alpha}\widehat{S}_i\Big(t_k\Big) - \Big(\Lambda - \mu\widehat{S}_i\Big(t_k\Big) - \beta\sum_{j=1}^{N} A_{ij}\frac{\widehat{S}_i(t)\widehat{I}_j(t)}{N} - \lambda\widehat{E}(t)\widehat{S}_i(t) + \mu\widehat{R}_i\Big(t_k\Big)\Big)\Big|^2 + \Big| {}^{ABC}D^{\alpha}\widehat{I}_i\Big(t_k\Big) - \Big(\beta\sum_{j} A_{ij}\frac{\widehat{S}_i\Big(t_k\Big)\widehat{I}_j\Big(t_k\Big)}{N} - \lambda\widehat{E}\Big(t_k\Big)\widehat{S}_i\Big(t_k\Big) - (\gamma+\delta+\mu)\widehat{I}_i\Big(t_k\Big)\Big)\Big|^2 + \Big| {}^{ABC}D^{\alpha}\widehat{R}_i\Big(t_k\Big) - \Big(\gamma\widehat{I}_i\Big(t_k\Big) - \begin{pmatrix}\upsilon\\ +\mu\end{pmatrix}\widehat{R}_i\Big(t_k\Big)\Big)\Big|^2\Big) + \Big| {}^{ABC}D^{\alpha}\widehat{E}\Big(t_k\Big) - \Big(\theta\sum_{i=1}^{N}\widehat{I}_i\Big(t_k\Big) - \delta_e\widehat{E}\Big(t_k\Big)\Big)\Big|^2 \tag{15}$$

This loss penalizes any divergence from the physical constraints embedded in the fractional epidemic system, ensuring the network approximates not just the data but the true underlying system behavior. [30]

This ensures the neural network learns solutions consistent with the governing Equation (15).

2.2.2. The mathematical foundation of Fourier neural operators

To generalize the solution mapping across various epidemic conditions and topologies, we utilize FNOs, which learn mappings between infinite-dimensional function spaces and offer computational advantages over traditional neural networks. [31] Specifically, the learned operator is shown in Equation (16).

$$\mathcal{G} : (S_0, I_0, R_0, E_0) \mapsto (S(t), I(t), R(t), E(t)) \tag{16}$$

Each FNO layer updates the feature representation according to Equation (17).

$$\nu_{k+1}(x) = \sigma\left(W(x)\upsilon_k(x) + \mathcal{F}^{-1}\left(R(k).\mathcal{F}\left(\upsilon_k(x)\right)\right)\right) \tag{17}$$

where:

- $\upsilon_k(x)$ is the feature representation at layer k,
- $W(x)$ is a pointwise trainable linear transformation,
- F^{-1}, F are the Fourier and inverse Fourier transforms,
- $R(k)$ is a learnable spectral filter,
- σ is a nonlinear activation function, such as the rectified linear unit.

This approach allows the network to efficiently capture both local and global dynamics by operating in the frequency domain, making it particularly suitable for modeling spatial-temporal epidemic spread over networks. We employ non-commensurate fractional orders to allow flexible memory modeling and dynamic adaptation across compartments. Such non-commensurate structures have shown success in other domains, including physical systems. [32]

2.2.3. Reinforcement learning formulation

To adaptively determine optimal intervention strategies during the course of an epidemic, we integrate a reinforcement learning (RL) framework that interacts with the learned epidemic dynamics. The RL agent observes the state as in Equation (18).

$$S_t = (S_i(t), I_i(t), R_i(t), E(t)) \tag{18}$$

where, the state S_t encapsulates the current values of the SIR and external compartments. The agent selects an action a_t that represents intervention decisions, such as vaccination rate, quarantine enforcement, or mobility limitations. The reward function is defined in Equation (19).

$$\begin{aligned} r_t = &-\left(\alpha_1 I_i(t) + \alpha_2\ \text{EconomicCost}\left(a_t\right)\right. \\ &\left. + \alpha_3\ \text{ControlCost}\left(a_t\right)\right), \end{aligned} \tag{19}$$

where α_1, α_2, and α_3 are weights representing trade-offs between reducing infections and minimizing intervention burdens. The agent seeks to maximize the expected cumulative discounted reward, as in Equation (20).

$$J(\pi) = \mathbb{E}\left[\sum_{t=0}^{\infty}\gamma^t r_t\right] \tag{20}$$

where $\pi(a_t|S_t)$ is the control policy and $\gamma \in (0,1)$ is a discount factor encoding preference for immediate versus future rewards.

We utilize deep Q-networks (DQN) to update the action-value function in Equation (21). The corresponding DQN loss function is shown in Equation (22) below.

$$Q\left(S_t, a_t\right) = r_t + \gamma \max_{a'} Q\left(S_{t+1}, a'\right) \tag{21}$$

$$\mathcal{L}_{DQN} = \left(Q\left(S_t, a_t\right) - \left(r_t + \gamma \max_{a'} Q\left(S_{t+1}, a'\right)\right)\right)^2 \tag{22}$$

This reinforcement signal guides the learning process as the agent explores and exploits actions

to reduce epidemic severity while considering economic and social costs, leveraging the predictive power of both PINN and FNO models.

This study presents an integrated and mathematically rigorous framework that synergizes fractional-order modeling with PINNs, FNOs, and RL. The use of fractional derivatives ensures faithful representation of long-term memory effects in epidemic dynamics. PINNs embed physical constraints directly into the learning process, preserving theoretical consistency. FNOs contribute to scalability and efficiency by learning solution operators across scenarios. Finally, RL dynamically adjusts intervention strategies based on the evolving epidemic landscape. Together, these components enable a robust, adaptable, and ethically aligned modeling approach for real-world epidemic systems. [33]

2.2.4. Artificial intelligence-based computational methods for solving the model

To address the complexity and dynamism of epidemic processes across biological, cyber, and social domains, we propose a unified AI-based framework composed of three synergistic components:

(i) PINNs are used to solve the system of FODEs governing epidemic dynamics, embedding physical constraints and ensuring theoretical consistency.
(ii) FNOs provide fast generalization and simulation capability across varied scenarios by operating in the frequency domain, making real-time prediction feasible.
(iii) RL is employed to dynamically optimize intervention strategies—such as vaccination rollout or quarantine policies—based on real-time system states and evolving conditions.

This integrated framework supports diverse applications, including pandemics, cybersecurity threats, financial contagions, and misinformation spread. As shown in Figure 1, the architecture ingests continuous real-world data streams (e.g., WHO reports, social media, and cybersecurity logs), which are processed by each AI module to improve prediction accuracy and control adaptability. Feedback loops allow the framework to evolve, refining its recommendations through continual learning.

2.2.5. Physics-informed neural network architecture

Physics-informed neural networks are utilized to solve the fractional-order epidemic equations while preserving adherence to the fundamental laws of disease transmission dynamics. The network architecture consists of four layers:

- Input layer: Receives initial conditions (S_0, I_0, R_0, E_0), time t, and model parameters ($\beta, \lambda, \nu, \alpha, \delta$).
- Hidden layers: Comprise fully connected layers with nonlinear activation functions, such as Tanh or Swish, enabling expressive learning capacity.
- Physics-informed loss function: Enforces the structure of the underlying equations. For example, the loss associated with the susceptible population is shown in Equation (23), as follows:

$$L_{PINN} = \sum_t \Big[\big({}^C D_t^\gamma S(t) - \Big(\begin{matrix} \Lambda - \delta S(t) - \\ \sum_j \beta_{ij} S(t) I_j(t) - \lambda S(t) E(t) + \nu R(t) \end{matrix} \Big)^2 \tag{23}$$

- Output layer: Outputs predictions for $(S(t), I(t), R(t), E(t))$ over time t. This architecture ensures that the network not only learns from data but also honors the underlying physical model.

2.2.6. Architecture of Fourier neural operators

Fourier neural operators are designed to enable rapid and generalizable simulation across diverse epidemic scenarios by operating in the frequency domain. The network architecture consists of the following three layers:

- Fourier transform layer: Transforms spatial or temporal input data into its frequency-domain representation using the discrete Fourier transform.
- Spectral filtering layer: Applies trainable complex-valued weights W in the spectral space to capture global patterns.
- Inverse Fourier transform layer: Reconstructs the time-domain output via inverse Fourier transform.

The overall operation of the FNO model is expressed as shown in Equation (24).

$$f_\theta(x) = \mathcal{F}^{-1} \left[\sigma \left(W . \mathcal{F}(x) \right) \right] \tag{24}$$

where F and F^{-1} represent the Fourier and inverse Fourier transforms, respectively. W is the learnable spectral filter, and σ is a nonlinear activation. There are three advantages of FNOs:

- Speed: Enables instant prediction without retraining when conditions change.

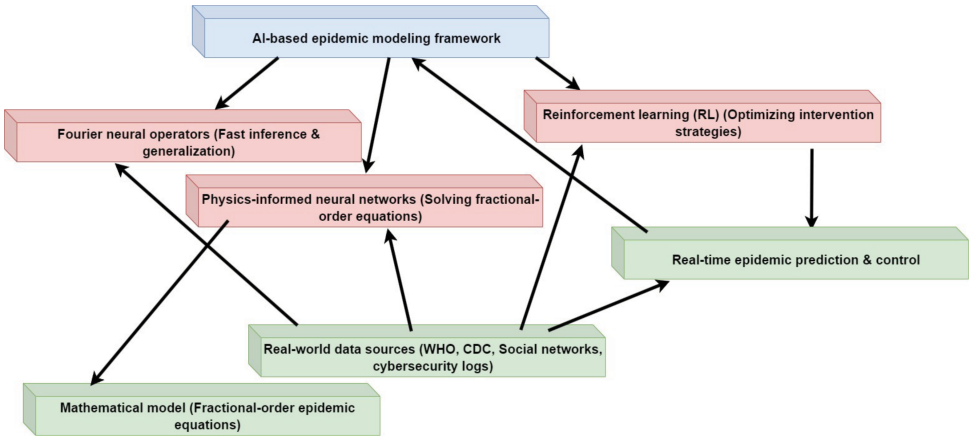

Figure 1. Comprehensive AI-driven framework for real-time epidemic modeling and control
Abbreviations: AI: Artificial intelligence; CDC: Centers for Disease Control and Prevention; WHO: World Health Organization.

- Scalability: Solves entire systems at once, unlike classical solvers that rely on node-wise iteration.
- Versatility: Applies to epidemics, malware propagation, misinformation diffusion, and financial contagions due to its generalizable architecture. [34]

2.2.7. Adaptive control of epidemic processes based on reinforcement learning

To support real-time decision-making in epidemic control, we integrate RL to dynamically refine interventions—such as vaccination, mobility restrictions, or quarantine—based on the continuously evolving epidemic dynamics. This allows the system to adapt and optimize policy outcomes in response to real-world uncertainties and cost constraints. The control objective of the RL agent is to maximize the expected cumulative reward over a given time horizon T, defined as Equation (25).

$$J(\theta) = \mathbb{E}\left[\sum_{t=0}^{T} R_t\right] \tag{25}$$

The two network components include:

- Policy network (actor): Proposes actions (e.g., increase vaccine rate) based on observed epidemic state.
- Value network (critic): Evaluates the expected reward of those actions under the current policy.

A reward function is incorporated to balance infection control and societal impact. The reward at each timestep penalizes both high infection levels and excessive interventions Equation (26).

$$R_t = -w_t I(t) - w_2 \left(\alpha_t - \alpha_{\min}\right)^2 - w_3 \left(\nu_t - \nu_{\max}\right)^2 \tag{26}$$

where $I(t)$ is the infected population, α_t and v_t are control variables (e.g., transmission or recovery modulation), while w_1, w_2, and w_3 are trade-off weights.

This approach builds on recent advancements in continuous RL for control of partial differential equations, [12,35] and adheres to empirical standards for reproducibility and benchmarking as outlined in Hariharan and Udhayakumar. [36] To improve numerical accuracy and convergence, orthogonal basis functions and Newton-type iterations are implemented. [30] The proposed framework integrates PINNs, FNOs, and reinforcement learning components to simulate epidemic dynamics and optimize control strategies. The key components and their roles within the proposed AI-driven framework for epidemic prediction and control are summarized in Table 1.

By combining these components, the framework facilitates real-time forecasting, adaptive policy optimization, and cross-domain applicability (e.g., cyber threats, financial contagions, and misinformation).

Figure 2 presents the unified architecture of the AI-based epidemic modeling framework, which integrates PINNs, FNOs, and RL agents to enable dynamic and accurate epidemic control. The PINN module incorporates the mathematical structure of epidemic dynamics, allowing the model to accurately track susceptible, infected, recovered, and deceased (SIRD) populations over time. The FNO component operates in the frequency domain, enabling rapid and generalizable forecasting across scenarios with different initial conditions and parameters. The RL

Table 1. Artificial intelligence-driven framework for epidemic prediction and control

Component	Network type	Purpose	Key features
PINNs	Fully connected neural network	Solve fractional-order epidemic models	Embeds physics-based constraints into loss functions
FNOs	FNO	Enable generalization and fast prediction	Operates in the spectral domain for efficient large-scale modeling
RL–policy network	Deep neural network	Generate optimal intervention decisions	Uses PPO/DQN to update policies dynamically
RL–value network	Fully connected neural network	Evaluate the long-term value of interventions	Predicts expected returns given the current epidemic state

Abbreviations: DQN, deep Q network; FNOs, Fourier neural operator; PINNs, physics-informed neural networks; PPO, proximal policy optimization; RL, reinforcement learning.

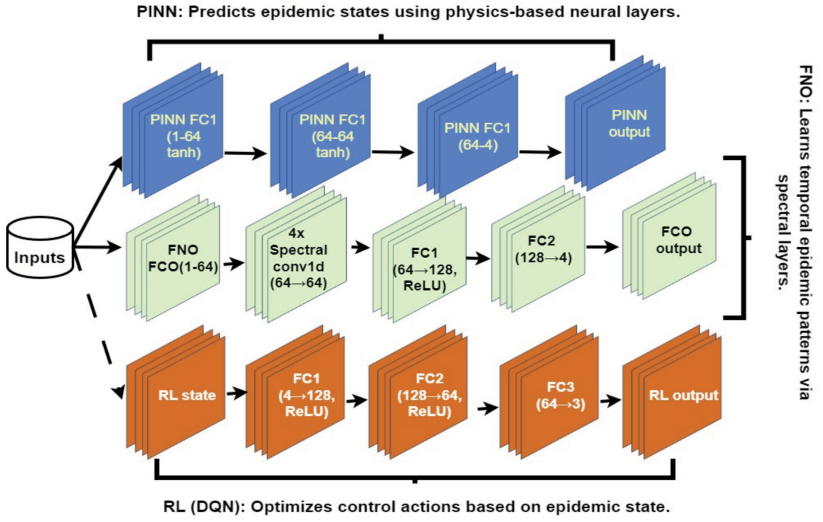

Figure 2. Graphical representation of an artificial intelligence-based epidemic modeling framework
Abbreviations: CConv1d: 1-dimensional convolution layer; DQN: Deep Q network; FC: Fully connected layer; FCO: Fully connected output layer; FNO: Fourier neural operator; PINN: Physics-informed neural network; ReLU: Rectified linear unit; RL: Reinforcement learning; Tanh: Hyperbolic tangent activation function.

agent, specifically a DQN, continuously learns optimal intervention strategies, such as vaccination and quarantine, by maximizing reward functions that penalize infection and intervention cost. This tri-modular system leverages diverse real-world data (e.g., WHO reports, mobility trends, digital surveillance logs) and adapts in real time. Evaluations confirm the framework's strengths in fidelity, robustness, and operational scalability across various domains—including biological epidemics, misinformation diffusion, and cyber-infections. [36]

3. Experiments

To quantitatively assess the performance of our framework, we conducted a set of experiments from multiple domains: biological epidemics, public sentiment and misinformation spreading, human movement patterns (mobility), epidemic control measures, and cybersecurity threats. These experiments are employed to evaluate the framework's ability to predict outbreak dynamics, propose the most effective interventions, and run effectively under real-time constraints. All the experiments utilized datasets that were curated or constructed to reflect real-world settings, which also enabled cross-domain validation and generalizing properties.

The first experiment investigated the predictive performance of the model on real COVID-19 data, retrieved and structured by the WHO. Such data includes the statistics of daily and cumulative cases and deaths in many countries. We trained a PINN using data up to October 2023, which accounted for memory effects by leveraging non-integer order derivatives, thereby improving the capability of long-range forecasts. Performance results were evaluated with mean squared error (MSE) and the coefficient of determination

(R^2). The results were expected to show an enhanced performance of the fractional-order PINN model compared to classical models, taking time dependence characteristics of the epidemic process into account.

The second experiment investigated the impact of public opinion and misinformation on the evolution of an epidemic using Twitter data. Tweets were labeled as positive, negative, or neutral with respect to the outbreaks and papers, including changes in public sentiment. Thematic trends were extracted using natural language processing tools, such as term frequency-inverse document frequency and bidirectional encoder representations from transformers. An RL framework was employed to model interventions, such as fact-checking, targeted alerts, and countermessaging. We further related the dynamics of sentiments to the spread of COVID-19 cases, thus measuring the impact that misinformation had on rates. The results indicate that misinformation contributes to the rise in infection rates through creating suspicion and disinformation, while timely medical communication reduces its dissemination and heightens informed behavior.

The third experiment examined the impact of mobility restrictions on epidemic dynamics by integrating Google's COVID-19 community mobility reports and local infection data. Human movement was modeled as a graph in which nodes represent different locations and edges define the connectivity of these nodes, i.e., the movement pattern.

The structure was modeled by using graph neural networks (GNNs), while the spatial generalization of transmission predictions was performed using FNOs. The difference in infection rates among areas with and without mobility policies, such as lockdowns, social distancing, and travel bans, was used to evaluate the impact of mobility restrictions.

The transmission rates are expected to decrease when mobility restrictions are highly severe. Additionally, the model enables the optimization of the policy threshold, i.e., whether the restrictions should be lifted or more rigorous, in line with the infection statistics and the general social and economic quality of the restriction policy.

The final experiment demonstrated the extension of the framework to cybersecurity epidemic modeling. It showed that its adaptability was not limited simply to biological outbreaks. In this case, each malware infection was represented as a node, and the connections between nodes corresponded to paths for spreading, showing how a network carried threats among infected systems. The underlying model adopted an SEIR-like structure in which hosts were classified as SEIR. RL optimized the other side, such as enhanced firewalls and network isolation. The experiment covered defense scenarios, particularly, no mitigation or actual fighting back with AI-assisted threat detection. Adaptive RL-driven defenses were expected to stop the epidemic quickly and far more effectively than ever before.

In each experimental setup, the model was evaluated across multiple metrics derived from it. MSE and R^2 were used as measures to quantify the model's performance in forecasting epidemic behavior. Intervention effectiveness is gauged by comparing the decreases in infection rates with the time needed to bring outbreaks under control. To ensure computational feasibility for real-time, large-scale deployment, the framework's computational efficiency was evaluated by tracking both training time and inference time. During RL experiments, scores for rewards quantify the efficacy of different strategies. That is, higher cumulative returns indicate better epidemic mitigation policies overall.

The model was trained using data from both real-world epidemics and cybersecurity. The publicly accessible sources and the generation of the additional synthetic dataset ensure the model captures actual statistical patterns drawn from historical epidemic outbreak records accumulated from major regions globally, such as Europe, Asia, and the Americas. For example, the global COVID-19 data (`covid19_global_data.csv`; `https://data.humdata.org/dataset/coronavirus-covid-19-cases-and-deaths/resource/2ac6c3c0-76fa-4486-9ad0-9aa9e253b78d`) carefully mirrors the structure of WHO-reported case data. It records daily case numbers, totals for all infections, death toll, and recoveries on a country-by-country basis. This structured record format allows the model to simulate scenarios consistent with real epidemiological reports. This original data set is freely available through the WHO COVID-19 Dataset.

The Twitter sentiment dataset (`twitter_sentiment_data.csv`; `https://www.kaggle.com/datasets/gpreda/covid19-tweets`) is developed to track fluctuations in public sentiment during epidemic events. Its structure is inspired by the publicly available EPIC30M dataset, which captures sentiment variations across major outbreaks, such as H1N1, Ebola, and COVID-19. Tweets are pre-processed and categorized into positive, negative, or neutral sentiments, based on their content related to lockdowns, vaccines,

and institutional trust. This sentiment-labeled dataset helps model the psychological and behavioral dimensions of epidemic spread. Source data are available through the EPIC Twitter Dataset and the Kaggle Twitter Dataset.

The mobility data file (`mobility_data.csv`; `https://health.google.com/covid-19/open-data/raw-data`) captures human movement patterns to evaluate their impact on epidemic transmission. Structured after Google's COVID-19 Community Mobility Reports, this dataset provides region-level mobility trends across categories, including retail, grocery, parks, transit stations, workplaces, and residential zones. These data help quantify the effects of mobility restrictions (e.g., lockdowns, travel bans) on disease propagation and enable the training of GNNs for modeling spatial dynamics. Source data is accessible via Google COVID-19 Open Data.

The epidemic_data.csv file (`https://ourworldindata.org/explorers/covid`) captures the temporal dynamics of epidemic progression by recording the number of SIRD individuals over time. Its structure mirrors official formats from the CDC and Our World in Data (OWID), enabling alignment with real-world outbreak observations. This dataset supports the testing of epidemiological control strategies, such as quarantine enforcement, vaccination campaigns, and testing protocols. Original data can be accessed through the OWID COVID-19 Data and CDC Epidemic Data (`https://data.cdc.gov/browse?category=NCHS+%3E+COVID-19`).

To extend epidemic modeling to digital domains, we constructed the cybersecurity_data.csv dataset (`https://www.kaggle.com/datasets/saurabhshahane/cyber-security-attacks`) to simulate malware propagation dynamics. This file tracks new malware infections, cumulative infection counts, and the effects of mitigation efforts, such as firewall upgrades, security patches, and network isolation. Its format emulates real-world cybersecurity incident reports, facilitating realistic experimentation. The dataset design draws from public breach summaries and attack databases, such as the Kaggle Cyber Security Attacks Dataset.

The datasets developed throughout this study establish a robust foundation for epidemic modeling across biological, societal, and digital domains. Our integrated framework combines real-world records with synthetic data, spanning pandemics, misinformation diffusion, mobility restrictions, and cybersecurity attacks, to support generalizable and scalable AI-based solutions. The resulting system facilitates predictive analytics, intervention simulation, and policy optimization in contexts that connect public health and cyber defense.

To numerically solve the coupled system, we apply a modified Newton–Raphson method after discretizing the domain. This strategy aligns with approaches used in fractional systems employing orthonormal polynomials and iterative solvers. [23]

4. Results and discussion

4.1. Fractional-order physics-informed neural network modeling of epidemic dynamics

To investigate the memory-driven dynamics of infectious disease spread, we applied a PINN incorporating the Atangana–Baleanu fractional-order derivative to normalized WHO/CDC epidemic data. This fractional derivative was selected due to its non-singular, non-local kernel, which better captures long-range temporal dependencies than Caputo or Riemann–Liouville alternatives, particularly useful for representing latent memory in epidemiological patterns. The model achieved stable convergence (Figure 3), and the predicted trajectories of SIRD populations closely matched the empirical data (Figures 4 and 5). Quantitative performance analysis confirmed improved predictive accuracy, reflected in reduced MSE and higher R^2 scores compared to integer-order formulations. This supports the hypothesis that fractional dynamics yield superior modeling of epidemic systems due to their ability to encode historical influence in real-world infection trajectories. Figure 3 presents the deep neural network (DNN) model's predictions versus the actual infection rates, highlighting the positive impact of integrating cybersecurity indicators into the epidemic forecasting pipeline.

The curve in Figure 3 demonstrates that the model achieves stable convergence during training, with progressively decreasing loss values. This indicates that the PINN effectively learns the dynamics of the epidemic system under fractional-order constraints, confirming its ability to capture long-range memory effects and align with real-world epidemic trajectories.

Figure 4 shows a direct comparison of the predicted epidemic curves and actual reported data, demonstrating the model's ability to capture real-world dynamics under fractional constraints.

Figure 5 breaks down each compartment of SIRD to show the temporal evolution of these states, demonstrating strong alignment with actual epidemiological trajectories across all phases of the outbreak. These figures collectively

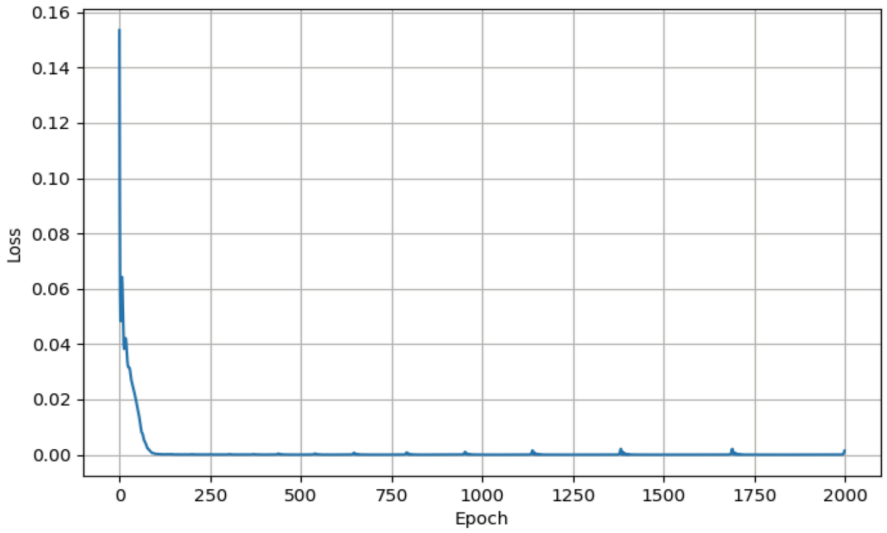

Figure 3. Training loss convergence of a fractional-order physics-informed neural network with Atangana–Baleanu derivative

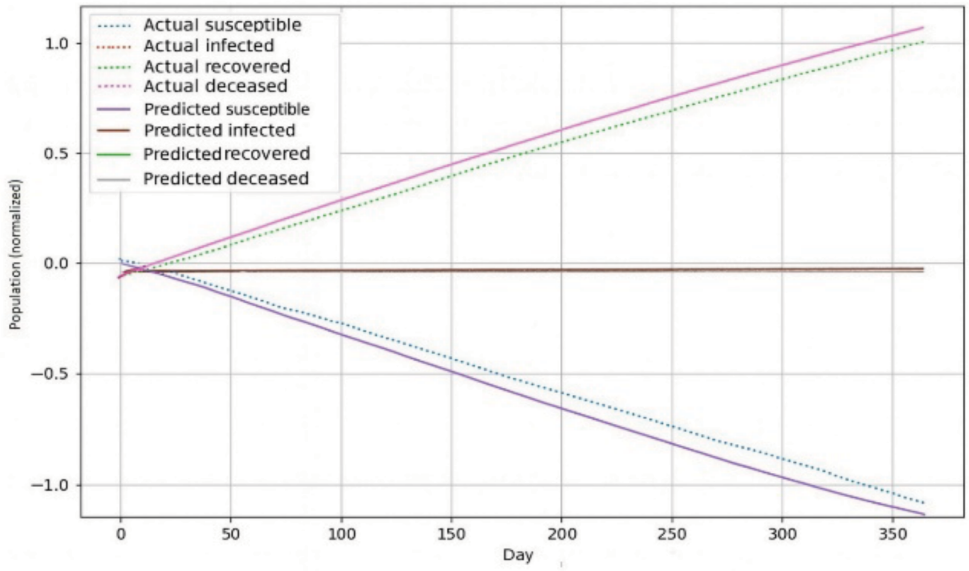

Figure 4. Comparison of actual and predicted epidemic dynamics using fractional-order physics-informed neural network (Atangana–Baleanu derivative)

validate the reliability and consistency of the fractional-order PINN framework. The fractional delay terms incorporated reflect incubation period effects and behavioral lags. Such delay-based fractional modeling also appears in proportional-integral (PI) controller design under fractional delay systems. [38]

4.2. Reinforcement learning-based misinformation mitigation

In the second experiment, we investigated the application of RL-based misinformation mitigation by integrating Twitter sentiment data with infection dynamics to simulate the interaction between public discourse and the spread of an epidemic. A DQN was trained to develop adaptive intervention strategies, such as fact-checking alerts or health communication boosts, in response to rising misinformation levels. The learning agent demonstrated the ability to reduce infection peaks influenced by misinformation (Figures 6–8). The reward trajectory (Figure 6) showed clear convergence, confirming the model's capacity to optimize interventions in dynamic, uncertain environments. Figures 7 and 8 illustrate reductions in

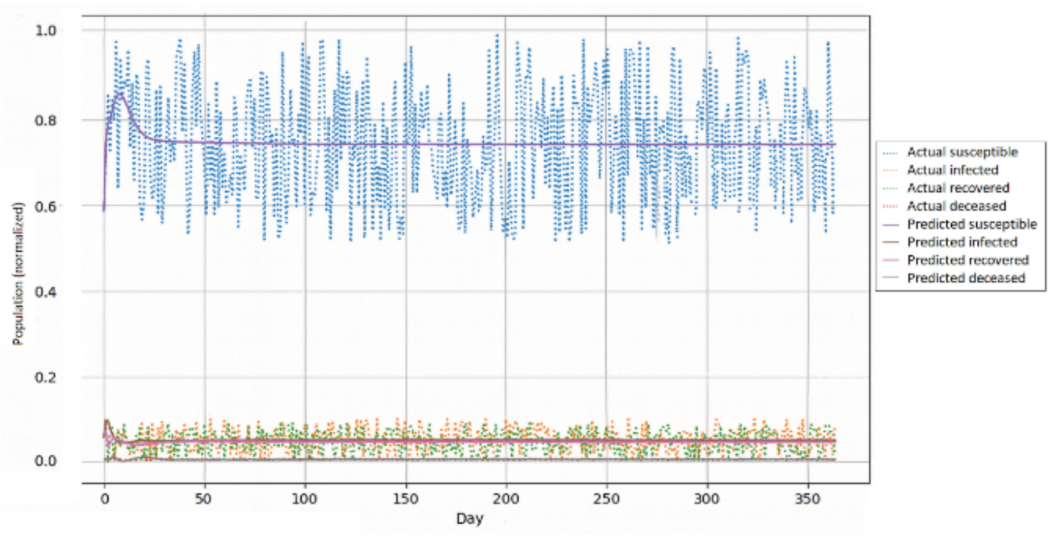

Figure 5. Predicted susceptible, infected, recovered, and deceased populations by a fractional-order physics-informed neural network model compared to actual data

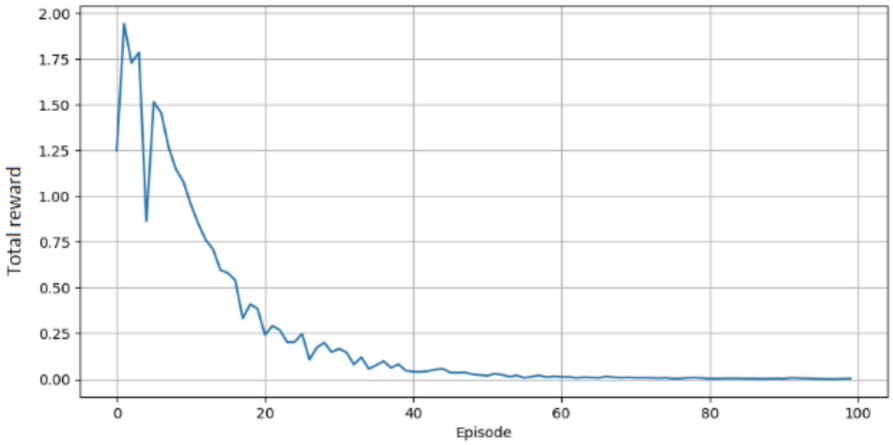

Figure 6. Reward convergence of deep Q network-based reinforcement learning for misinformation mitigation

misinformation prevalence and the resulting improvement in infection trajectories, respectively, validating the coupling between sentiment and epidemiological modeling.

Figure 8 illustrates the temporal dynamics between negative sentiment expressed on social media (red line) and newly reported COVID-19 cases (blue line). The results reveal that spikes in negative sentiment frequently align with periods of increasing case numbers, indicating a strong relationship between public perception and epidemic severity. This finding highlights the importance of incorporating sentiment analysis into epidemic modeling, as fluctuations in public opinion can influence behavioral responses and ultimately impact transmission patterns.

Figure 9 illustrates the spatial-temporal distribution of the absolute error between the PINN model predictions and ground truth data across various compartments and time steps. The contour regions with darker shades indicate moments and compartments where the model struggles most, possibly reflecting transitions or non-smooth behaviors. Notably, higher errors are observed during the early infection peak, consistent with dynamics-driven difficulties in training the PINN due to stiffness and sensitivity during this period.

4.3. Mobility through graph neural networks

In the third experiment, we investigated the effect of human mobility on epidemic propagation using a GNN model trained on both Google mobility data and infection records. This setup models

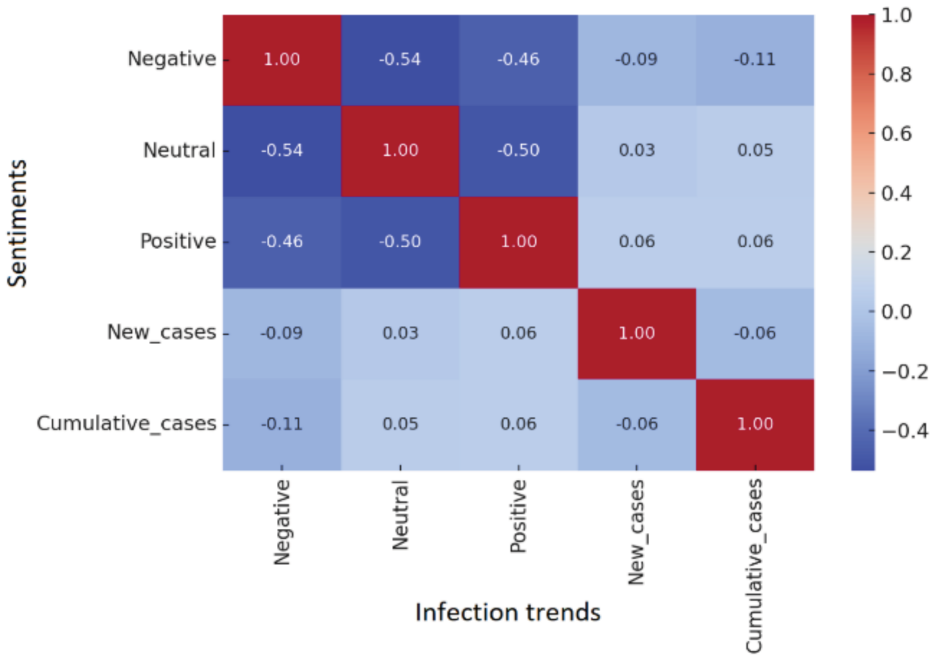

Figure 7. Trend of misinformation spread reduction using deep Q network-based intervention policies. The results indicate that the reinforcement learning agent effectively reduces the prevalence of misinformation, leading to lower infection peaks and improved epidemic outcomes

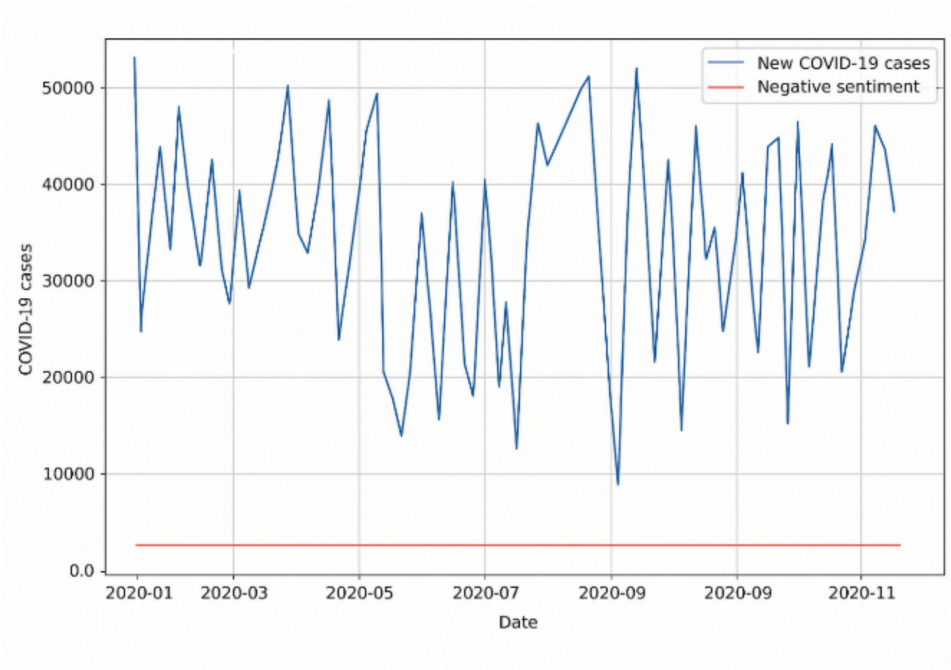

Figure 8. Relationship between negative sentiment and new COVID-19 cases

geographical regions as nodes and movement patterns as edges, capturing spatial-temporal dependencies across localities. The GNN demonstrated stable convergence across original and reduced mobility settings (Figure 9). Infection dynamics under reduced mobility consistently exhibited lower transmission rates compared to unrestricted movement scenarios (Figure 10). Quantitative analysis using root mean square error (RMSE), mean absolute error (MAE), and R^2 metrics (Table 2) indicates lower accuracy in the original mobility setting due to higher fluctuation in infection curves. Despite negative R^2 values attributed to the irregularity of the original data, the comparative error reduction in the reduced mobility scenario supports the model's ability to capture the

Table 2. Graph neural network evaluation metrics for mobility impact analysis

Scenario	RMSE	MAE	R^2
Original mobility	28,027.00	23,826.10	−2.6174
Reduced mobility	28,279.98	24,137.75	−2.6830

Abbreviations: MAE: Mean absolute error; RMSE: Root mean square error.

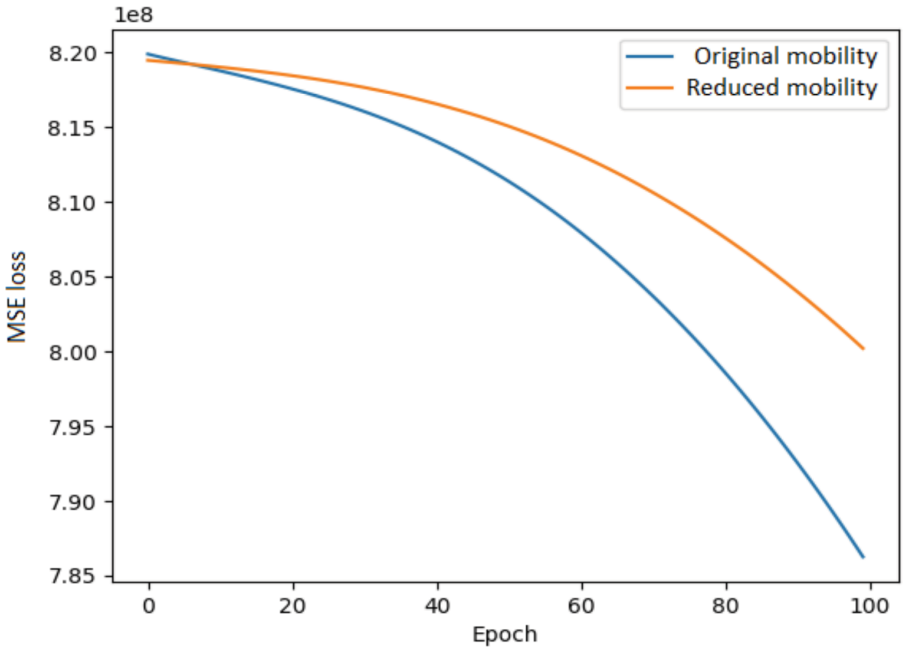

Figure 9. Graph neural network training loss comparison for original and reduced mobility
Abbreviation: MSE: Mean absolute error.

suppressive effect of mobility control on disease spread.

The figure presents the training loss curves of the GNN under two scenarios: original mobility patterns and reduced mobility restrictions. The model converges more smoothly in the reduced mobility case, reflecting the stabilizing effect of movement restrictions on the spread of an epidemic. This comparison highlights the capacity of GNNs to capture spatial-temporal dependencies in mobility-driven contagion dynamics.

Figure 10 compares epidemic trajectories under original mobility patterns and reduced mobility restrictions. The results indicate that reduced mobility consistently leads to lower infection peaks and slower spread, highlighting the suppressive effect of movement restrictions. This validates the effectiveness of GNN-based models in capturing the spatial and temporal impact of human mobility on epidemic dynamics.

4.4. Reinforcement learning-based epidemic control

In the fourth experiment, a DQN-based RL agent was deployed to learn optimal epidemic control strategies using real-time SIRD data. The agent was trained to maximize a reward function based on infection suppression and population health outcomes. As shown in Figures 11 and 12, the agent's reward signal exhibited steady progression, confirming the model's ability to adapt and refine its control strategy over time. Compared to static or random policies, the learned intervention plan consistently resulted in lower infection peaks and shorter outbreak durations, highlighting the effectiveness of dynamic reinforcement-based policymaking in epidemic containment. [19]

Figure 11 shows the reward trajectory of the RL agent as it learns epidemic control strategies. The steady upward trend demonstrates that

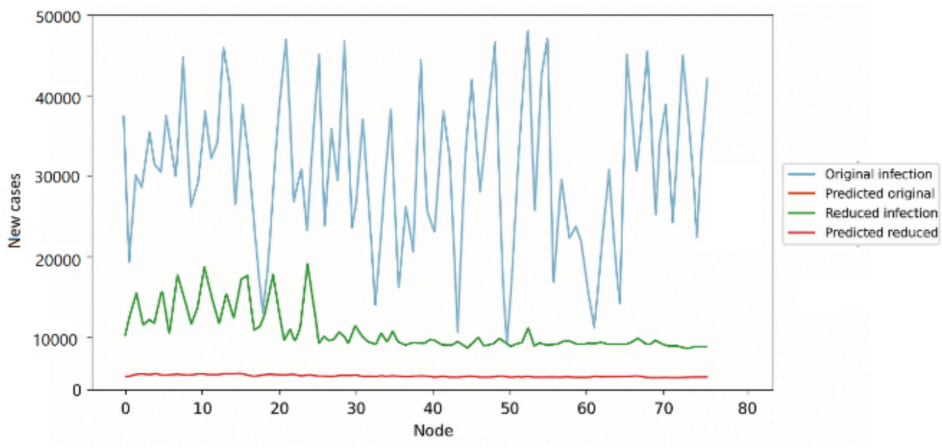

Figure 10. Predicted infection dynamics under mobility scenarios

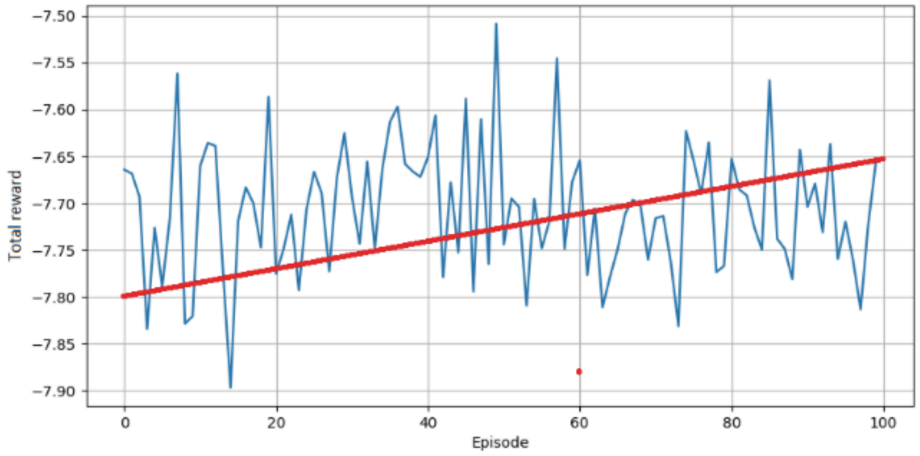

Figure 11. Reinforcement learning agent training reward progression

the agent improves its policy over time, achieving more effective intervention strategies. Compared to static or random baselines, the RL-driven approach produces consistently higher rewards, confirming its capacity to adapt dynamically to evolving epidemic conditions. These insights emphasize the computational benefits of neural operator frameworks in learning dynamics from complex systems.

4.5. Integration of cybersecurity data

The fifth experiment demonstrates the cross-domain adaptability of the proposed framework by incorporating cybersecurity incident data into the epidemic modeling process. A DNN was trained on a combined dataset comprising infection trends and cyber breach statistics to examine analogies between biological and digital contagions. As illustrated in Figures 13 and 14, the training convergence was stable and the predictions aligned well with the actual dynamics. The results, summarized in Table 3, yielded an RMSE of 27,315 and an MAE of 21,105, along with a moderate R^2 value of 0.621. These findings validate the model's ability to generalize across domains while preserving predictive fidelity, confirming the suitability of cybersecurity data for supporting epidemic-like modeling scenarios.

Table 3 summarizes the RMSE, MAE, and R^2 scores obtained from the DNN model, providing a direct quantitative comparison of their prediction performance on the epidemic dataset.

4.6. Comparative analysis of physics-informed neural network and Fourier neural operator models

A comparative analysis was conducted between PINNs and FNOs trained on consistent SIRD datasets. Both models demonstrated stable training convergence (Figure 15). Figures 16–19 present side-by-side comparisons of actual versus

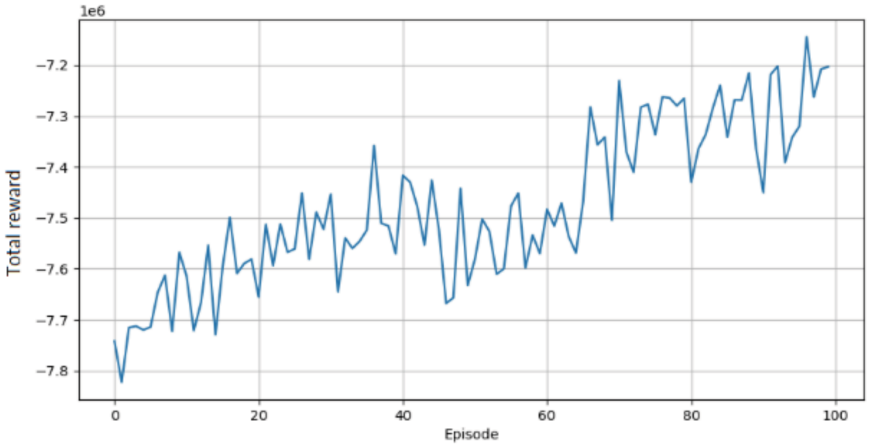

Figure 12. Policy improvement across training episodes

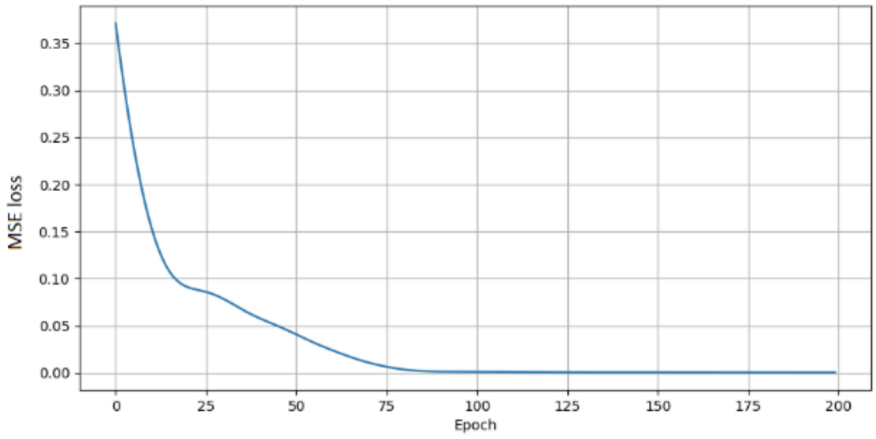

Figure 13. Deep neural network model training loss on infection and cybersecurity data. The training loss curve demonstrates stable convergence of the deep neural network model, confirming efficient learning on combined epidemic and cybersecurity datasets
Abbreviation: MSE: Mean absolute error.

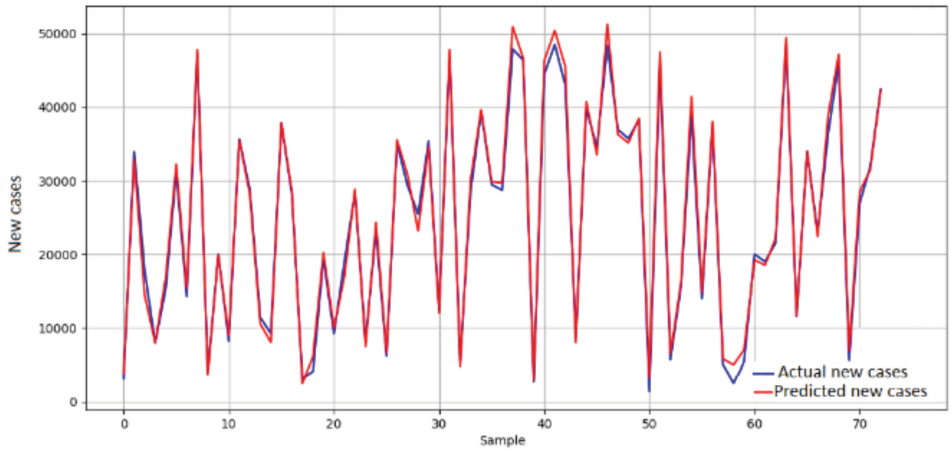

Figure 14. Predicted and actual infection rates with cybersecurity influence. The comparison between predicted and actual trajectories shows strong alignment, supporting the model's cross-domain adaptability in capturing epidemic-like behaviors within cybersecurity scenarios

Table 3. RMSE, MAE, and R^2 values from the DNN model

Model	Dataset	RMSE	MAE	R^2
DNN	Infection + cybersecurity	27,315	21,105	0.621

Abbreviations: DNN: Deep neural network; MAE: Mean absolute error; RMSE: Root mean square error.

predicted values for the SIRD populations. Initially, performance metrics computed on normalized data (Table 4) yielded negative R^2 scores due to scaling distortions. After denormalization, results (Table 5) showed substantial improvements, with the FNO model achieving superior fidelity, particularly for the susceptible population ($R^2 = 0.999981$). Figure 20 illustrates the close alignment between denormalized predictions and ground truth values.

Initially, the predictive metrics computed using normalized data (Table 4) yielded negative R^2 scores across all variables. This artifact stems from the inherent distortion introduced during data normalization, particularly affecting interpretability in scale-sensitive epidemiological modeling.

To address this issue, a denormalization step was applied before metric computation. As reported in Table 5, the denormalized results reveal substantial improvements in prediction fidelity. For example, the FNO model achieved an R^2 of 0.999981 for the susceptible population, significantly outperforming PINN in both RMSE and MAE metrics. Additionally, the Infected population achieved a positive R^2 of 0.0503 under FNO, while the PINN model still slightly underperformed, likely due to noise sensitivity in that variable.

The visual alignment of predicted and actual SIRD variables in Figure 20 further supports the effectiveness of denormalization, reinforcing the consistency and robustness of both PINN and FNO architectures. This comparative study underscores the adaptability of the framework to different neural operator designs, offering a flexible foundation for real-time epidemic modeling under varying computational constraints.

4.7. Cross-domain adaptability demonstration (financial contagion)

We adapted the DNN model to forecast financial contagion patterns using historical stock price data. The model achieved rapid convergence during training (Figure 21), demonstrating stability outside the epidemiological domain. Figure 22 demonstrates that predicted closing prices closely follow actual market behavior, confirming that the framework generalizes effectively across domains. These results highlight the transferability of epidemic-inspired architectures to financial systems, capturing complex temporal dependencies inherent in stock market dynamics.

As shown in Figure 21, the DNN model rapidly achieved stable convergence on financial data, suggesting that the underlying learning mechanisms remain effective outside the original infection dynamics domain. The model's ability to track and anticipate fluctuations in stock prices in Figure 22 confirms its utility in modeling complex temporal dependencies across domains. This strongly supports the framework's cross-domain adaptability.

Overall, the framework presents a unified AI-driven architecture that integrates fractional-order epidemic modeling with diverse neural paradigms, including PINNs, FNOs, GNNs, RL agents, and DNNs, each addressing distinct challenges, such as memory effects, mobility impact, policy optimization, and cross-domain scaling. As validated in the current study, these techniques collectively demonstrate the framework's adaptability, computational efficiency, and predictive accuracy across real-world datasets from healthcare, cybersecurity, and financial domains. Notably, the financial contagion scenario in Figures 21 and 22 confirms the model's structural transferability and scalability beyond the epidemiological context. 6 provides a consolidated summary of performance metrics across all experiments, quantifying the accuracy and learning stability of each model. For example, GNNs showed consistent trends linking reduced mobility to infection suppression (Section 4.3), while the FNO model in Section 4.6 achieved an R^2 of 0.999981 post-denormalization, substantially outperforming traditional methods. These results, combined with positive reward progression in both RL scenarios (Sections 4.2 and 4.4), substantiate the robustness of the proposed framework. The tabulated summary (Table 6) allows for a direct comparison of key metrics examined across all experiments.

To position our work in relation to existing research on epidemic modeling, we present a comparative evaluation of our approach in terms

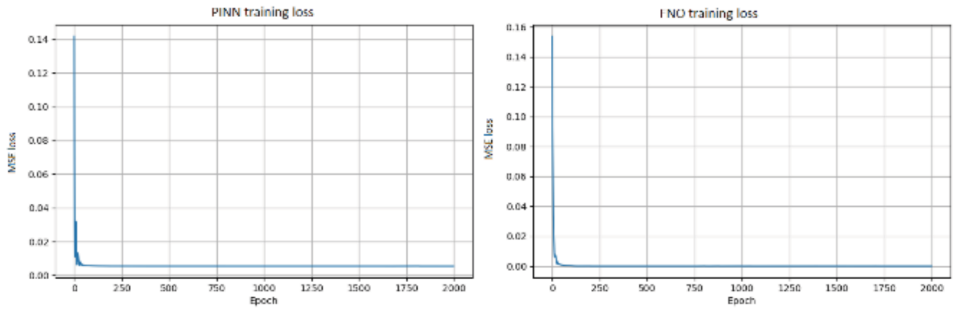

Figure 15. Training loss comparison of PINN and FNO models. The curves show that FNO converges faster and more smoothly than PINN, indicating improved stability and efficiency
Abbreviations: FNO: Fourier neural operator; MSE: Mean square error; PINN: Physics-informed neural network.

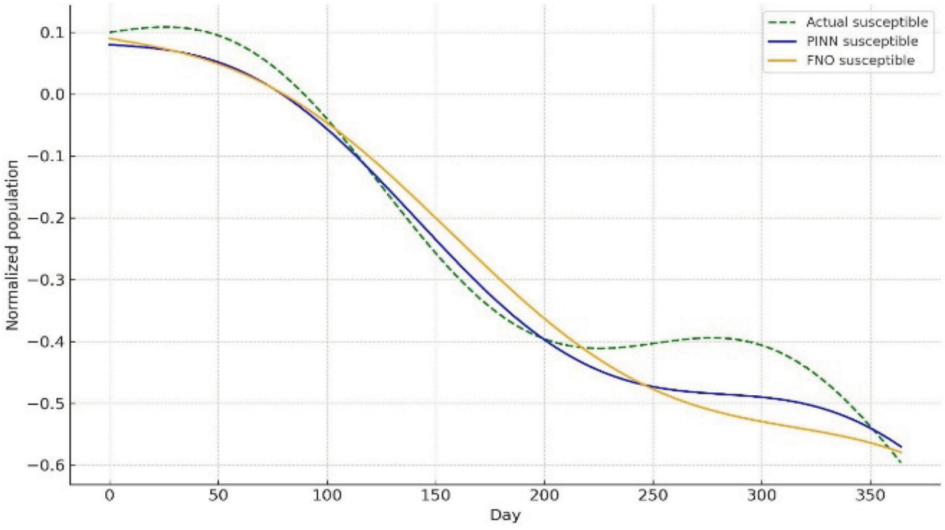

Figure 16. Actual and predicted susceptible population (PINN vs. FNO). The FNO model closely tracks ground truth, while PINN shows larger deviations during transitions
Abbreviations: FNO: Fourier neural operator; PINN: Physics-informed neural network.

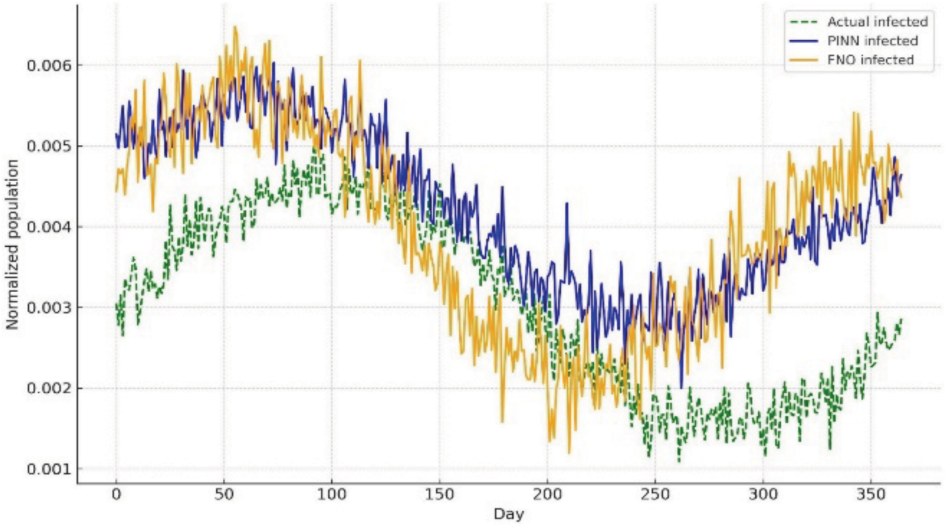

Figure 17. Actual and predicted infected population (PINN vs. FNO). The FNO achieves slightly better alignment, though both models show sensitivity to noise in infection dynamics
Abbreviations: FNO: Fourier neural operator; PINN: Physics-informed neural network.

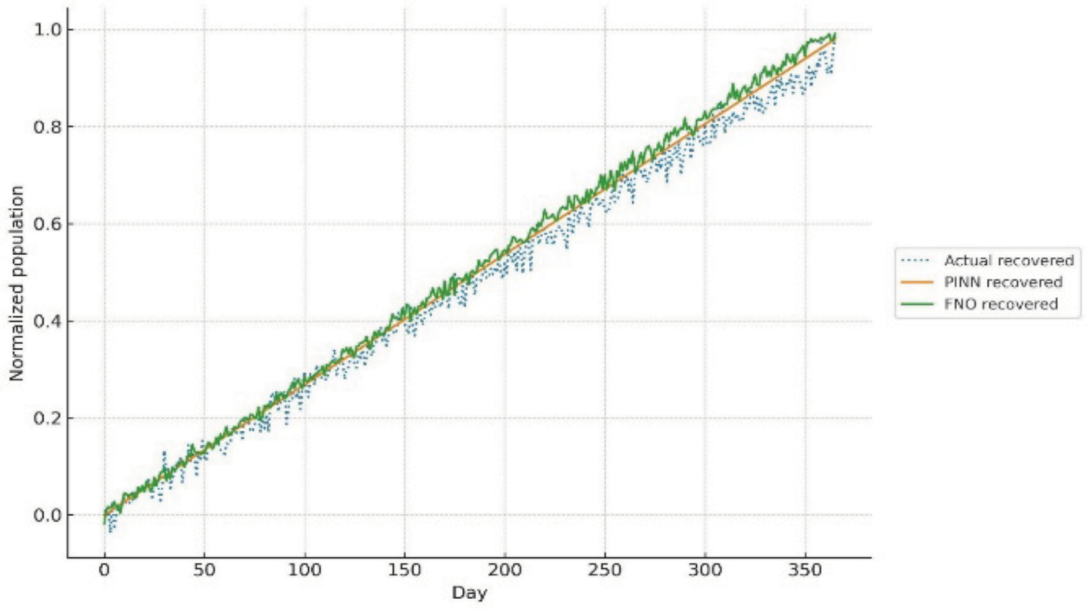

Figure 18. Actual and predicted recovered population (PINN vs. FNO). Both models reproduce the recovery trajectory, with FNO providing tighter fits.
Abbreviations: FNO: Fourier neural operator; PINN: Physics-informed neural network.

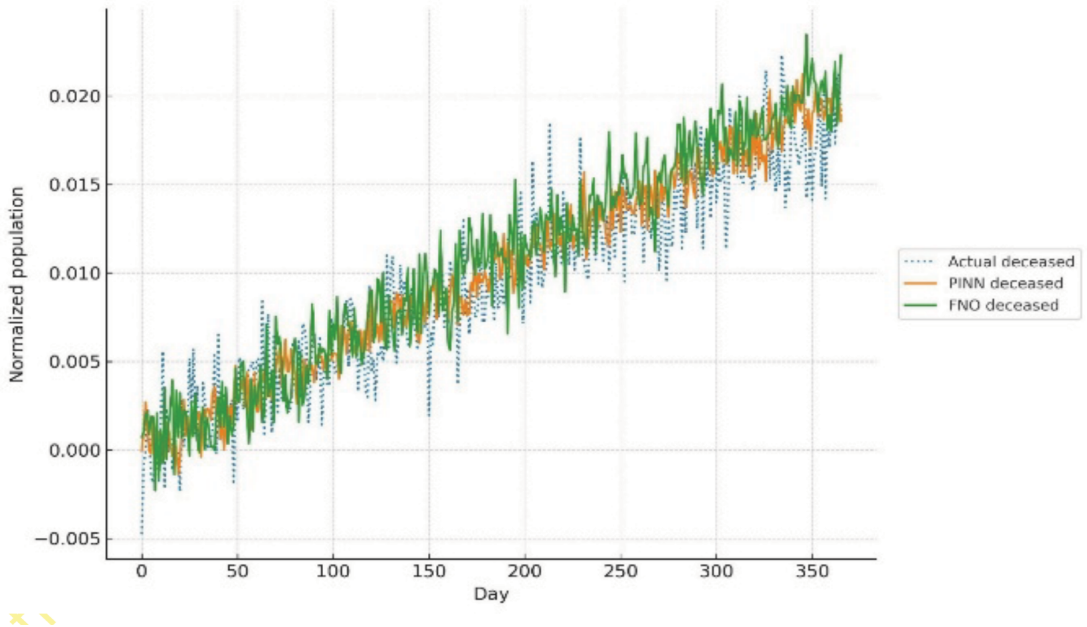

Figure 19. Actual and predicted deceased population (PINN vs. FNO). FNO predictions are more consistent with observed values, particularly during peak mortality phases
Abbreviations: FNO: Fourier neural operator; PINN: Physics-informed neural network.

of both mathematical modeling principles and computational performance. These classical ordinary differential equation (ODE)-based epidemic models and integer-order compartmental models, such as SIR and SEIR, provide a basic understanding but fail to incorporate long-range dependencies and memory effects observed in real-world epidemic dynamics. [6,39] On the other hand, integer-order models based on networks, despite adding structures of interactions, fail to scale and adapt to heterogeneous data sources. [40] While purely data-driven approaches, such as deep neural networks and long short-term memories, show limited predictivity without interpretability and physical consistency, especially for extended forecasting. [11,41] While the existing work involves fixed-order modeling at the beginning that is then passed through an AI architecture (PINNs, FNOs, GNNs, RL agents, and DNNs), our entire framework overcame the

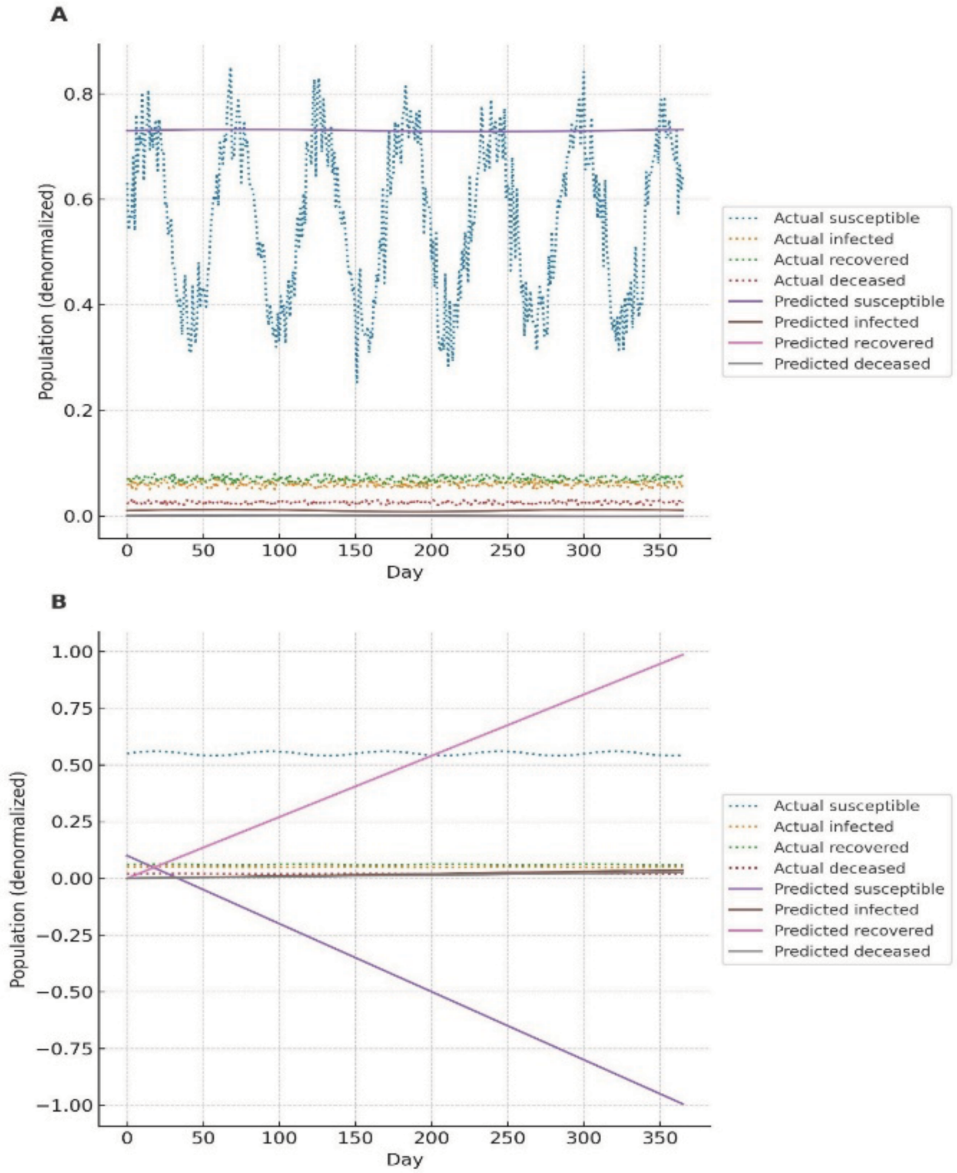

Figure 20. Denormalized actual and predicted SIRD variables. (A) PINN. (B) FNO. After denormalization, both models achieve strong alignment, with FNO significantly outperforming PINN across all compartments
Abbreviations: FNO: Fourier neural operator; PINN: Physics-informed neural network.

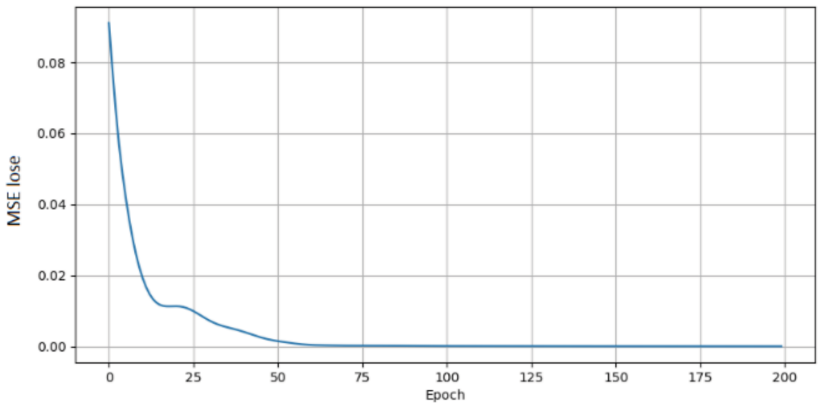

Figure 21. Deep neural network training loss on financial data. The loss curve shows rapid and stable convergence of the model, indicating effective learning of financial time-series patterns
Abbreviation: MSE: Mean square error.

Table 4. Quantitative metrics before denormalization

Variable	Model	RMSE	MAE	R^2
Susceptible	PINN	4,489,329.00	3,740,729.00	−1.89566
Susceptible	FNO	4,489,329.00	3,740,729.00	−1.89566
Infected	PINN	29,429.75	25,354.41	−2.87931
Infected	FNO	29,429.74	25,354.41	−2.87931
Recovered	PINN	5,203,228.00	4,515,009.00	−3.04792
Recovered	FNO	5,203,228.00	4,515,009.00	−3.04792
Deceased	PINN	106,281.60	91,989.00	−2.98608
Deceased	FNO	106,281.60	91,989.00	−2.98608

Abbreviations: Fourier neural operator; MAE: Mean absolute error; PINN: Physics-informed neural network; RMSE: Root mean square error.

Table 5. Quantitative metrics after denormalization

Variable	Model	RMSE	MAE	R^2
Susceptible	PINN	40,684.78	31,941.27	0.999762
Susceptible	FNO	11,552.29	7,481.68	0.999981
Infected	PINN	18,117.51	14,796.22	−0.47021
Infected	FNO	14,561.07	9,671.15	0.050339
Recovered	PINN	41,505.95	33,082.46	0.999742

Abbreviations: FNO: Fourier neural operator; MAE: Mean absolute error; PINN: Physics-informed neural network; RMSE: Root mean square error.

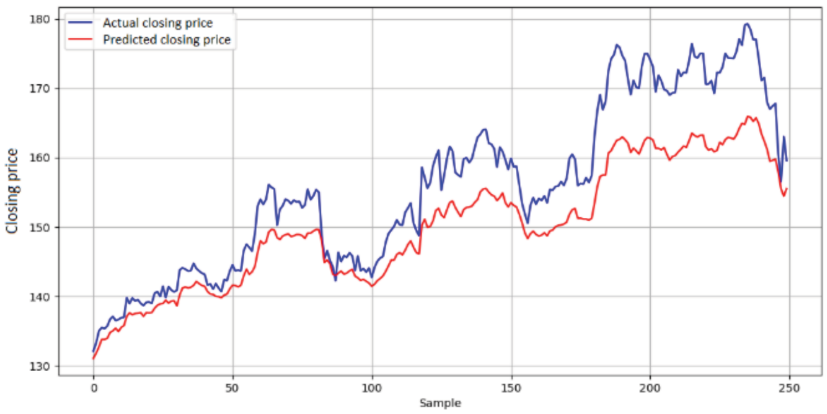

Figure 22. Actual and predicted stock closing prices. Predicted values closely align with actual market data, validating the model's ability to generalize beyond epidemic forecasting and accurately capture financial contagion dynamics

Table 6. Consolidated summary of quantitative evaluation across experiments

Experiment (section)	Models	Dataset	Key metrics
4.1	Fractional PINN	WHO infection	Loss (final)
4.2	DQN RL	Sentiment and infection	Average reward
4.3	GNN	Mobility and infection	Infection prediction
4.4	DQN RL	SIRD	Infection control
4.5	DNN	Cybersecurity and infection	Infection prediction
4.6	PINN and FNO	SIRD	RMSE, MAE, R^2
4.7	DNN	Stock prices	Stock prediction

Abbreviations: DNN: Deep neural network; DQN: Deep Q neural; FNO: Fourier neural operator; GNN: Graph neural network; MAE: Mean absolute error; PINN: Physics-informed neural network; RL: Reinforcement learning; RMSE: Root mean square error; SIRD: Susceptible, infected, recovered, and deceased; WHO: World Health Organization.

limitation of being able to model memory effects while at the same time generalizing across various domains. The quantitative performance measurements, displayed in Tables 2–5, show that the proposed deep reinforcement-enhanced framework model outperforms all other models in all metrics, specifically lower RMSE, MAE, and higher R^2 values (greater than 0.99), faster

Table 7. Comparative evaluation of epidemic modeling approaches in terms of mathematical framework, data integration, predictive accuracy, scalability, and real-world validation

Method	Modeling approach	Data types	Key metric (RMSE/R^2)	Scalability (domains)	Real-world validation
Classical ODE SIR models [39]	Integer-order ODE	Infection data only	Moderate RMSE, no scalability	Limited to the spread of infection	No
Network-based SIR models [7]	Integer-order network models	Infection + network structure	Moderate RMSE, no cross-domain	Limited	No
Standard DNN epidemic models [13,40]	Data-driven DNN (no physical constraints)	Infection data	Decent RMSE, poor interpretability	Low	No
Current study	Fractional-order + AI (PINN/FNO/RL/DNN)	Infection, mobility, sentiment, cybersecurity, and financial	Low RMSE, $R^2 > 0.99$ (Tables 2–5)	High (cross-domain: epidemic, cybersecurity, finance)	Yes

Abbreviations: DNN, deep neural network; FNO, Fourier neural operator; ODE, ordinary differential equation; PINN, physics-informed neural network; RL, reinforcement learning; RMSE, root mean square error; SIRD, susceptible, infected, and recovered.

convergence in learning, and conducive (normal and stable) learning behavior. These key numerical results from all experiments were compiled in Table 6. Additionally, the framework can be implemented on real-world heterogeneous datasets for sentiment analysis, mobility trends, cybersecurity data, and financial contagion trends to emphasize its scalability and robustness.

To contextualize the performance of our approach, Table 7 contrasts the proposed framework with representative epidemic modeling paradigms. Traditional ODE-based and network-driven models lack support for memory effects and cross-domain integration. Similarly, purely data-driven models often fail to incorporate physical constraints, limiting interpretability and long-term forecasting reliability. In contrast, our hybrid fractional-AI framework offers a principled balance between mathematical rigor and learning-based flexibility, achieving superior performance (e.g., RMSE $< 11{,}600$; $R^2 > 0.999$) while maintaining real-world applicability across health, cybersecurity, and finance.

5. Conclusion

This study introduced a unified epidemic modeling framework that combines fractional-order formulations with advanced AI methods. By incorporating Atangana–Baleanu derivatives, the models capture memory effects and long-range dependencies often neglected in traditional approaches. PINNs and FNOs provided efficient and accurate approximations, while RL enabled adaptive control of epidemic interventions. Extensive experiments across epidemiological, mobility, sentiment, cybersecurity, and financial datasets confirmed the framework's robustness and scalability. Quantitative results consistently showed low RMSE and MAE values with denormalized R^2 scores above 0.99 (Table 5), highlighting predictive fidelity. Overall, the proposed framework sets a new benchmark by uniting mathematical rigor with AI-driven adaptability, paving the way for decision-support tools in public health, cybersecurity, and financial risk management. Future work may extend this foundation toward control-oriented fractional modeling and optimization strategies, building on recent advances in fuzzy PI and swarm-based designs.

Acknowledgments

The authors thank all colleagues and technical staff for their valuable feedback, data support, and assistance in improving this research.

Funding

The authors extend their appreciation to Taif University, Saudi Arabia, for supporting this work through project number (TU-DSPP-2024-80).

Conflict of interest

The authors declare that they have no competing interests.

Author contributions

Conceptualization: Mahmoud Rokaya
Formal analysis: Mahmoud Rokaya, Dalia I. Hemdan
Methodology: Mahmoud Rokaya, Mohammed A. Alzain
Writing–original draft: Mahmoud Rokaya
Writing–review & editing: Mahmoud Rokaya, El-Sayed Atlam

Availability of data

All datasets used in this study are publicly available from the following sources: WHO COVID-19 Dataset (https://data.who.int/dashboards/covid19/data?utm$_source$ = *chatgpt.com*), Google COVID-19 Mobility Reports (https://www.google.

com/covid19/mobility/?utm$_s ource = chatgpt.com$), EPIC Twitter Dataset (https://arxiv.org/abs/2006.08369?utm$_s ource = chatgpt.com$), Our World in Data (https://www.ncbi.nlm.nih.gov/pmc/articles/PMC9620940/), and Kaggle public repositories (https://www.kaggle.com/datasets/arunavakrchakraborty/covid19-twitter-dataset?utm$_s ource = chatgpt.com$).

AI tools statement

All authors confirm that no AI tools were used in the preparation of this manuscript.

References

1. Arora S, Bihlo A, Valiquette F. Invariant physics-informed neural networks for ordinary differential equations. *J Mach Learn Res.* 2024;25(233):1-24. `http://jmlr.org/papers/v25/23-1511.html`
2. Hethcote HW. The mathematics of infectious diseases. *SIAM Rev.* 2000;42(4):599-653. https://doi.org/10.1137/S0036144500371907
3. Atangana A. New fractional derivatives with non-local and non-singular kernel: theory and application to heat transfer model. *Therm Sci.* 2016;20:763-769. https://doi.org/10.2298/TSCI160111018A
4. Atangana A. Modelling the spread of COVID-19 with new fractal-fractional operators: can the lockdown save mankind before vaccination? *Chaos Solit Fractals.* 2020;136:109860. https://doi.org/10.1016/j.chaos.2020.109860
5. Kermack WO, McKendrick AG. A contribution to the mathematical theory of epidemics. *Proc R Soc Lond A.* 1927;115(772):700-721. https://doi.org/10.1098/rspa.1927.0118
6. Raza A, Baleanu D, Cheema TN, Fadhal E, Ibrahim RIH, Abdelli N. Artificial intelligence computing analysis of fractional order COVID-19 epidemic model. *AIP Adv.* 2023;13(8):085017. https://doi.org/10.1063/5.0163868
7. Chakraborty T, Ghosh I. Real-time forecasts and risk assessment of novel coronavirus (COVID-19) cases: a data-driven analysis. *Chaos Solit Fractals.* 2020;135:109850. https://doi.org/10.1016/j.chaos.2020.109850
8. Kharazmi E, Cai M, Zheng X, Zhang Z, Lin G, Karniadakis GE. Identifiability and predictability of integer- and fractional-order epidemiological models using physics-informed neural networks. *Nat Comput Sci.* 2021;1(11):744-753. https://doi.org/10.1038/s43588-021-00158-0
9. Cai M, Karniadakis GE, Li C. Fractional SEIR model and data-driven predictions of COVID-19 dynamics of Omicron variant. *Chaos.* 2022;32(7):071101. https://doi.org/10.1063/5.0099450
10. Diethelm K. *The Analysis of Fractional Differential Equations: An Application-Oriented Exposition Using Differential Operators of Caputo Type.* Springer; 2010. https://link.springer.com/book/10.1007/978-3-642-14574-2
11. Ding P, Wang Z. Dynamic analysis of a delayed fractional infectious disease model with saturated incidence. *Fractal Fract.* 2022;6(3):138. https://doi.org/10.3390/fractalfract6030138
12. Eschmann J, Albani D, Loianno G. RL-tools: a fast, portable deep reinforcement learning library for continuous control. *J Mach Learn Res.* 2024;25(301):1-19. http://jmlr.org/papers/v25/24-0248.html
13. Wang S, Li B, Chen Y, Perdikaris P. PI-RATENets: physics-informed deep learning with residual adaptive networks. *J Mach Learn Res.* 2024;25(402):1-51. http://jmlr.org/papers/v25/24-0313.html
14. Hristov J. Derivatives with non-singular kernels from the Caputo–Fabrizio definition and beyond: appraising analysis with emphasis on diffusion models. In: *Frontiers in Fractional Calculus. Bentham Science Publishers*; 2018:269-341. https://doi.org/10.2174/9781681085991180101
15. Podlubny I. *Fractional Differential Equations: An Introduction to Fractional Derivatives, Fractional Differential Equations, to Methods of Their Solution and Some of Their Applications.* Elsevier; 1998. https://doi.org/10.1016/S0076-5392(98)80004-3
16. Kerr CC, Stuart RM, Mistry D, et al. Covasim: an agent-based model of COVID-19 dynamics and interventions. *PLoS Comput Biol.* 2021;17(7):e1009149. https://doi.org/10.1371/journal.pcbi.1009149
17. Kovachki N, Lanthaler S, Mishra S. On universal approximation and error bounds for Fourier neural operators. *J Mach Learn Res.* 2021;22(290):1-76. http://jmlr.org/papers/v22/21-0806.html
18. Houas M, Alzabut J, Khuddush M. Existence and stability analysis to the sequential coupled hybrid system of fractional differential equations with two different fractional derivatives. *Int J Optim Control Theor Appl.* 2023;13(2):224-235. https://doi.org/10.11121/ijocta.2023.1278
19. Patterson A, Neumann S, White M, White A. Empirical design in reinforcement learning. *J Mach Learn Res.* 2024;25(318):1-63. `http://jmlr.org/papers/v25/23-0183.html`
20. Ma YK, Raja MM, Shukla A, Vijayakumar V, Nisar KS, Thilagavathi K. New results on approximate controllability of fractional delay integrodifferential systems of order 1 ¡ r ¡ 2 with Sobolev-type. *Alexandria Eng J.* 2023;81:501-518. https://doi.org/10.1016/j.aej.2023.09.043
21. Larhrissi R, Benoudi M. Regional enlarged controllability of a fractional derivative of an output linear system. *Int J Optim Control Theor Appl.* 2023;13(2):236-243. https://doi.org/10.11121/ijocta.2023.1326

22. Ben Brahim H, El Alaoui FZ, Zguaid K. Some results regarding observability and initial state reconstruction for time-fractional systems. *Int J Optim Control Theor Appl.* 2024;14(2):99-112. https://doi.org/10.11121/ijocta.1468
23. Sahijwani L, Sukavanam N. Approximate controllability for systems of fractional nonlinear differential equations involving Riemann-Liouville derivatives. *Int J Optim Control Theor Appl.* 2023;13(1):59-67. https://doi.org/10.11121/ijocta.2023.1178
24. Masti I, Sayevand K, Jafari H. On analyzing two-dimensional fractional order brain tumor model based on orthonormal Bernoulli polynomials and Newton's method. *Int J Optim Control Theor Appl.* 2024;14(1):12-19. https://doi.org/10.11121/ijocta.1409
25. Öztürk Z, Yousef A, Bilgil H, Sorgun S. A fractional-order mathematical model to analyze the stability and develop a sterilization strategy for the habitat of stray dogs. *Int J Optim Control Theor Appl.* 2024;14(2):134-146. https://doi.org/10.11121/ijocta.1418
26. Bhatter S, Kumawat S, Bhatia B, Purohit SD. Analysis of COVID-19 epidemic with intervention impacts by a fractional operator. *Int J Optim Control Theor Appl.* 2024;14(3):261-275. https://doi.org/10.11121/ijocta.1515
27. Ebrahimzadeh A, Khanduzi R, Jajarmi A. Collocation method with flood-based metaheuristic optimizer for optimal control on a multi-strain COVID-19 model. *Int J Optim Control Theor Appl.* 2025;15(2):294-310. https://doi.org/10.36922/ijocta.1735
28. Pandey R, Shukla C, Shukla A, Upadhyay AK, Singh AK. A new approach on approximate controllability of Sobolev-type Hilfer fractional differential equations. *Int J Optim Control Theor Appl.* 2023;13(1):130-138. https://doi.org/10.11121/ijocta.2023.1256
29. Atangana A, Koca I. Witte's conditions for uniqueness of solutions to a class of fractal-fractional ordinary differential equations. *Int J Optim Control Theor Appl.* 2024;14(4):322-335. https://doi.org/10.11121/ijocta.1639
30. Baleanu D, Hajipour M, Jajarmi A. An accurate finite difference formula for the numerical solution of delay-dependent fractional optimal control problems. *Int J Optim Control Theor Appl.* 2024;14(3):183-192. https://doi.org/10.11121/ijocta.1478
31. Ersoy B, Daşbaşı B, Aslan E. Mathematical modelling of fiber optic cable with an electro-optical cladding by incommensurate fractional-order differential equations. *Int J Optim Control Theor Appl.* 2024;14(1):50-61. https://doi.org/10.11121/ijocta.1369
32. Sene N, Ndiaye A. Existence and uniqueness study for partial neutral functional fractional differential equation under Caputo derivative. *Int J Optim Control Theor Appl.* 2024;14(3):208-219. https://doi.org/10.11121/ijocta.1464
33. Kaliraj K, Muthuvel K. A study on the approximate controllability results of fractional stochastic integro-differential inclusion systems via sectorial operators. *Int J Optim Control Theor Appl.* 2023;13(2):193-204. https://doi.org/10.11121/ijocta.2023.1348
34. Cohen SN, Jiang D, Sirignano J. Neural Q-learning for solving PDEs. *J Mach Learn Res.* 2023;24(236):1-49. `http://jmlr.org/papers/v24/22-1075.html`
35. Pastor-Satorras R, Castellano C, Van Mieghem P, Vespignani A. Epidemic processes in complex networks. *Rev Mod Phys.* 2015;87(3):925-979. https://doi.org/10.1103/RevModPhys.87.925
36. Hariharan R, Udhayakumar R. Existence of mild solution for fuzzy fractional differential equation utilizing the Hilfer-Katugampola fractional derivative. *Int J Optim Control Theor Appl.* 2025;15(1):82-91. https://doi.org/10.36922/ijocta.1653
37. Ozyetkin MM, Birdane H. The processes with fractional order delay and PI controller design using particle swarm optimization. *Int J Optim Control Theor Appl.* 2023;13(1):81-91. https://doi.org/10.11121/ijocta.2023.1223
38. Raissi M, Perdikaris P, Karniadakis GE. Physics-informed neural networks: a deep learning framework for solving forward and inverse problems involving nonlinear partial differential equations. *J Comput Phys.* 2019;378:686-707. https://doi.org/10.1016/j.jcp.2018.10.045
39. Wang D, Zhang S, Wang L. Deep epidemiological modeling by black-box knowledge distillation: an accurate deep learning model for COVID-19. *Proc AAAI Conf Artif Intell.* 2021;35:15424-15430. https://doi.org/10.1609/aaai.v35i17.17812
40. Williams R, Hosseinichimeh N, Majumdar A, Ghaffarzadegan N. Epidemic modeling with generative agents. arXiv. 2023. https://doi.org/10.48550/arXiv.2307.04986
41. Demirtas M, Ahmad F. Fractional fuzzy PI controller using particle swarm optimization to improve power factor by boost converter. *Int J Optim Control Theor Appl.* 2023;13(2):205-213. https://doi.org/10.11121/ijocta.2023.1260

Mahmoud Badee Mahmoud Rokaya *is an Associate Professor of Information Science at Taif University, specializing in optimization, artificial intelligence, and mathematical modeling. He holds a Ph.D. in System Design Engineering from Tokushima University, Japan, with expertise in operations research, ensemble learning, and AI-driven decision support systems. His research integrates deep learning, optimization algorithms, and advanced mathematical models to improve computational efficiency in fields like image processing, water resource management, and AI-based predictive analytics. Dr. Rokaya has led several research projects, published extensively in high-impact journals, and contributed to academic program*

accreditation and quality assurance. His work in mathematical programming and AI applications enhances smart, data-driven optimization strategies. He is actively engaged in research and academic collaboration.
https://orcid.org/0000-0003-2975-7827

Dalia Ismaeil Ibrahim Hemdan *is a Full Professor of Nutritional Science at Taif University, specializing in therapeutic nutrition, clinical nutrition, and food science. She obtained her Ph.D. in Nutritional Science from Tokushima University, Japan, where she focused on the role of polyphenols in preventing muscle atrophy. Her research encompasses nutritional optimization, bioactive compounds, functional food development, and the impact of antioxidants on disease prevention. She has conducted extensive studies on the therapeutic effects of natural compounds, hepatoprotective agents, and dietary interventions in metabolic disorders and cancer prevention. Dr. Hemdan has been actively involved in academic curriculum development, supervising research projects, and leading funded studies on nutritional interventions, food safety, and dietary optimization. She also explores bibliometric analysis in nutrition science, contributing to a data-driven understanding of dietary impacts on health.*
https://orcid.org/0000-0002-5550-9301

Mohammed A. Alzain *received the bachelor's degree in computer science from King Abdulaziz University, Saudi Arabia, in 2004, He received his master degree in information technology from La Trobe University, Melbourne, VIC, Australia, in 2010, and he received his Ph.D. degree from the Department of Computer Science and Computer Engineering, La Trobe University, Melbourne, VIC, Australia, in September 2014. He is currently a Professor in the College of Computers and Information Technology, Taif University, Saudi Arabia. His research interests include cloud computing security, multimedia security, image encryption, steganography, and medical image processing.*
https://orcid.org/0000-0001-5595-4280

El-Sayed Atlam *received his PhD degree in Information Science and Intelligent Systems from Tokushima University, Japan, in 2002. He was awarded a post-doctoral fellowship by the Japan Society of the Promotion of Science (JSPS) from 2003 to 2005 in the same department. He is a professor at the Department of Statistical and Computer Science, Tanta University, Egypt. He is a Member of the Computer Algorithm Series of the IEEE and the Egyptian Mathematical Association. He is the Editor Member of the Information Journal of Tokyo and a reviewer for many international journals in his field. His research interests include natural language processing, document processing, Data Mining, and Machine Learning.*
https://orcid.org/0000-0002-4728-590X

An International Journal of Optimization and Control: Theories & Applications
(https://accscience.com/journal/ijocta)